This is to certify that the

thesis entitled

MECHANICAL PROPERTIES OF METALLIC-GLASS REINFORCED

GLASS-CERAMIC COMPOSITES

presented by

RAJENDRA UDDHAV VAIDYA

has been accepted towards fulfillment
of the requirements for

MASTERS degree in MATERIALS SCIENCE

K. N. Subramanian

Major professor

Date 2/23/88

MECHANICAL PROPERTIES OF METALLIC-GLASS REINFORCED GLASS-CERAMIC COMPOSITES

By

Rajendra Uddhav Vaidya

A THESIS

Submitted to
Michigan State University
in partial fulfillment of the requirements
for the degree of

MASTER OF SCIENCE

Department of Metallurgy, Mechanics and Materials Science

1988

ABSTRACT

MECHANICAL PROPERTIES OF METALLIC-GLASS REINFORCED GLASS-CERAMIC COMPOSITES

By

Rajendra Uddhav Vaidya

Glass-ceramic matrix composites, reinforced with a very low volume fraction of metallic-glass ribbons, were fabricated by conventional wet-pressing and sintering techniques. Even with a very low volume fraction of metglass ribbon reinforcements, high improvements in strength, elastic properties and fracture toughness were achieved, relative to the values of the brittle glass-ceramic matrix. The elastic properties of this composite system did not obey the rule of mixtures; although they satisfied the equations suggested by Halpin and Tsai[52]. Microcracking was observed at the edges of the reinforcing ribbons, and these microcracks improved the fracture toughness of the composite system. The flaw initiating failure was primarily in the tensile region of the matrix phase. The interfacial bond between the ribbon and the matrix, was found to be very strong. The thermal shock resistance of the composite specimens was not significantly different from that of the matrix.

ACKNOWLEDGEMENTS

First and foremost, I would like to thank my advisor Professor K. N. Subramanian for his valuable help and support over the course of this investigation. I would also like to extend my thanks to Dr. Drzal and the Composite Materials and Structures Center, Michigan State University for supporting this work. Special thanks are also due to Dr. Eldon Case, for his valuable help and suggestions. I would also like to thank Professor Kalinath Mukherjee and all other staff members and students of the Department of Metallurgy, Mechanics and Materials Science, for their timely help and support. Last but not least, I wish to thank my father Uddhav Vaidya, mother Vyjanthi Vaidya and sister Rajeshree Vaidya for their love, encouragement and support, without which this would not have been possible.

TABLE OF CONTENTS

Page

LIST OF TABLES.....iii

LIST OF FIGURES.....iv

EXPERIMENTAL PROCEDURES.....20

Specimen preparation.....20
Measurement of the elastic properties.....24
Strength measurements.....32
Thermal shock resistance testing.....34
Fracture toughness measurements.....36
Interfacial bond strength measurements.....44

RESULTS AND DISCUSSION.....48

Elastic properties.....48
Strength measurements.....55
Fractographic analysis.....65
Thermal shock resistance.....93
Fracture toughness measurement.....106
Interfacial bond strength.....110

CONCLUSIONS.....113

REFERENCES.....115

LIST OF TABLES

Table — Page

1. Properties of the metglass ribbon reinforcements....21
2. Properties of the matrix glasses.....23
3. Position of the nodes for various modes of vibration, in terms of fractions of the specimen length.....29
4. Values of the coefficients A_0, A_1, A_2, A_3 and A_4 for different bending configurations.....39
5. Elastic properties of the matrix and composite.....49
6. Comparison of the experimentally measured and theoretically calculated(rule of mixtures) values of Young's modulus.....51
7. Three point bend test results.....56
8. Comparison of the values of the Young's modulus obtained from the Dynamic Resonance test and Three point bend test.....64
9. Thermal shock resistance data (unreinforced 7572 matrix specimens).....94
10. Thermal shock resistance data (7572 matrix + 0.8% MT 2605/S-2 ribbons).....95
11. Results of the Notched Beam test used in the measurement of Fracture toughness.....107
12. Results of the Indentation technique used for the measurement of Fracture toughness.....108
13. MOR and midplane shear stress for the matrix and composite specimens.....112

LIST OF FIGURES

Figure Page

1. Experimental set-up for the Dynamic Resonance test....26

2. Specimen configuration in the Dynamic Resonance test....27

3. Experimental set-up for the Single Edge Notched Beam test....37

4. Variation in the shape factor(Y) with the ratio of crack deth(a) to specimen thickness(w)[46]....40

5. Length of crack(c) and semi-diagonal(a) of a Vicker's indentation....42

6. a) Schematic representation of stresses acting at the crack tip
   b) Crack tip at the ribbon interface
   c) Interface splitting and crack opening when the crack intersects the ribbon[51]....45

7. Experimental set-up for the pullout test....47

8. Variation in the Young's modulus of the composite with increasing volume fraction of metglass ribbon reinforcement....54

9. Stress-strain curves of the ribbon, matrix and composite....57

10. Variation in the fracture strength of the composite with increasing volume fraction of metglass ribbon reinforcement[53]....59

11. Variation in the experimentally determined fracture strength(MOR) of the composite, with increasing volume fraction of metglass ribbon reinforcement....62

12. General features observed on a fractured ceramic surface[55]....67

13. Hackle and mirror regions associated with a flaw....68

14. General features associated with a flaw....69

15. Flaw associated with the initiation of failure in the composite specimen.....70

16. Flaw associated with the initiation of failure in the composite specimen.....71

17. Strong interfacial bonding between the matrix and the ribbons. Some matrix material is observed to be adhering to the ribbon surface.....73

18. Matrix material adhering to the ribbon surface.....74

19. Strong(void free) bonding between the ribbons and the matrix. The matrix is observed to be 100% crystalline..... 75

20. Strong(void free) bonding between the ribbons and the matrix. The matrix is observed to be 100% crystalline.....76

21. Flaw at the ribbon-matrix interface.....77

22. Flaw at the ribbon-matrix interface.....78

23. Microcracks originating at the edges of the reinforcing ribbons.....80

24. Enlarged view of a region in Figure 23. Outward propagation of the microcracks can be observed in this figure.....81

25. Arrest of a crack by a metglass ribbon. The crack originated at the tensile surface during the bend test.....82

26. Enlarged view of a region in Figure 25. Crack arrest and deflection at the metglass ribbon-matrix interface can be observed in this figure.....83

27. Crack arrest at the ribbon-matrix interface.....84

28. Presence of a crushed zone at the ribbon-matrix interface.....86

29. Enlarged view of a region in Figure 28. The crushed zone at the ribbon-matrix interface can be clearly seen in this figure.....87

30. Enlarged view of a region in Figure 28.....88

31. Presence of a crushed one at the ribbon matrix interface.....89

32. Presence of a crushed one at the ribbon-matrix interface. Matrix material is observed to be adhering to the ribbon surface.....90

33. Vein type of fracture pattern on the metglass ribbon.....91

34. A crushed ribbon in composite failure.....92

35. Variation in the fracture strength(MOR) with severity of quench, for the unreinforced and composite specimens.....96

36. Percentage change in the Young's modulus of the unreinforced matrix specimens, with severity of quench.....97

37. Crack deflection into the tensile region of the thermally shocked specimens.....101

38. Crack deflection into the tensile region of the thermally shocked specimens.....102

39. Crack deflection into the tensile region of the thermally shocked specimens.....103

40. Crack deflection into the tensile region of the thermally shocked specimens.....104

41. Crack deflection and branching around the metglass ribbons in the thermally shocked specimens.....105

42. Variation in the Fracture toughness(K_{IC}) with increasing volume fraction of metglass ribbon reinforcement.....109

INTRODUCTION

A large number of modern applications of materials, especially in the field of Aerospace and Aeronautics, demand high temperature capabilities. Ceramics are being seriously considered as potential materials for these high temperature applications, because they have relatively higher melting points as compared to metals, and also retain their mechanical properties upto higher temperatures, as compared to metals. In addition, ceramics have lower densities and are more resistant to oxidation and corrosion as compared to metals. A majority of ceramics are also found abunduntly in nature.

The major drawback of ceramics, which has been inhibiting their widespread use, is their brittle nature, and tendency to fail catastrophically. For many years researchers have sought to develop methods to toughen ceramics, without losing their inherent qualities, such as high temperature strength and corrosion resistance. The addition of fibers to ceramics, has been known for many years as a means for approaching this goal. The developement of fiber-reinforced cement is undoubtedly the best known example. Extension of this concept to high performance ceramics is being pursued. The research done to date has proved that fiber-reinforcement is probably one of the best known techniques for improving the fracture

toughness of ceramics.

However, these composite ceramic materials are unlikely to be used in preference to simpler materials, unless there are substantial improvements to the material properties and performance. Another important factor which needs to be accounted for is the cost. The complex fabrication techniques required in the manufacture of ceramic composites, invariably increases the cost.

Fiber-reinforced ceramic matrix composites, have been proven to be a promising class of materials for applications where high strength, high stiffness, low thermal expansion, low density, low notch sensivity and high temperature environmental stability are desirable attributes, either singly or in combination. Experiments performed in England, Germany and the United States, as early as 1973[1-3], demonstrated the capabilities of fiber reinforced ceramics. Through the use of carbon fibers, glass matrix composites with strengths as high as 700 MPa were developed. Considerable advacement in fiber-reinforced ceramics have been made in recent years. Today, ceramic composites with strengths as high as 2000 MPa are being studied.

The properties of the composite depend to a very large extent on the properties of the components of the composite, namely the fiber and matrix. Selecting a fiber-matrix system, compatible with one another with respect to all their properties, is important. A large number of factors need to be taken into account, before selecting a suitable

fiber-matrix system. The matrix phase in practical systems, is likely to be an existing ceramic until new ceramic matrices are developed. Most of the conventional ceramics satisfy the basic requirements of high strength, good refractoriness and lightness. This is achieved through combinations of the light elements like boron, silicon, oxygen, nitrogen, aluminium, beryllium, carbon and magnesium. Most common ceramics contain more than one of these elements. Some of the conventional ceramics include alumina, silica, zirconia, silicon carbide, silicon nitride, various glasses and glass-ceramics.

The toughness and strength of monolithic ceramics can be improved considerably by the refinement of grain size. In addition, a number of mechanisms have been proposed to account for the increased toughness in certain ceramics; two of the most common modes are crack deflection and crack branching[4-6]. Cracks can be deflected by grain boundaries, second phase particles or by residual stress fields. The reorientation of the crack plane away from normal to the applied stress, causes a reduction in the crack driving force, with a subsequent increase in the fracture toughness.

Another proposed mechanism for the improvement in fracture toughness is that of microcracking[7]. Microcracking can be induced in ceramics in a number of ways, which include grinding, polishing and thermal shocking. Microcrack toughening arises from two crack tip

shielding processes; one due to the reduced elastic modulus of the microcracked body, and the other due to dilation induced due to microcracking.

Other mechanisms of toughening include transformation toughening in zirconia-based ceramics[8-10]. The martensitic transformation of zirconia, from its high temperature tetragonal structure to its room temperature monoclinic structure, is accompanyied by a 4% volume increase and a 7% shear distortion. The mechanism of transformation toughening is based on the stress induced matensitic transformation near the tip of the propagating crack. The toughening arises from a crack tip shielding process, in which the transformation strains cause a reduction in the crack tip stresses.

The theories proposed so far for the improved fracture toughness, are all based on the stress interactions occuring in the vicinity of the crack tip. However, recent studies[11] in large-grained alumina have indicated that other events taking place at large distances behind the crack tip are responsible for the improvement in the toughness. These studies include direct observation of secondary cracking and grain pullout. The proposed mechanism involves mechanical interlocking of the protruding grains on the rough fracture surfaces, which causes closure forces on the crack surfaces and hence a reduction in the stress intensity factor. Analysis of the problem has been hindered by the difficulty of determining the force-

displacement relation for the crack bridging forces.

Although the fracture toughness of monolithic ceramics has been improved through a number of mechanisms such as crack branching, crack deflection, transformation toughening etc, these ceramics still exhibit catastrophic failure, when the stored elastic strain energy exceeds the fracture energy. This is because of the low strain to failure in such brittle materials. The strain to failure in monolithic ceramics is usually of the order of 0.1-0.2%. Stronger the ceramic, higher is the notch sensitivity, and more catastrophic is the failure. On the other hand, ceramics reinforced with fibers exhibit a different failure mode, with much higher values of strain to failure.

In the case of monolithic ceramics, the tensile strength is used for predicting the engineering performance. In the case of composites, the assessment of the mechanical properties is a much more difficult task. This is because composites are usually anisotropic, either partly or wholely. A detailed fracture mechanics analysis has been recently developed for ceramic matrix composites[12]. The analysis is based on the observation that the fibers resist the opening of a matrix crack by frictional forces at the fiber-matrix interface. One of the important results of the analysis is that the stress required for matrix cracking is independant of the prexisting flaw size, and is therefore a material property.

The analysis also allows definition of the

microstructural changes that result in increased matrix cracking stress. However, there is a minimum value of cracking stress that can be obtained without causing a transition to a more brittle failure mode. In this mode, fiber failure accompanyies matrix cracking, resulting in the catastrophic failure of the composite. The transition occurs when the matrix cracking stress exceeds the fiber failure stress. The analysis has also been extended to this region of behaviour, but experimental confirmation is required.

Despite the various theories developed for characterizing the mechanical properties of ceramic matrix composites, a number of problems still exist. One of the difficulties arises from the non-unique relationship between the flaw size and fracture stress. The two parameters which strongly influence the fracture stress are inclusions and cracks. Surface cracks cause a maximum reduction in the strength and are dangerous. Considerable amount of information has been gained from studies of controlled model crack systems[13-15]. These controlled cracks are formed by loading a sharp hard indentor(Vickers or Knoop) onto the ceramic surface. This causes formation of half penny surface cracks, the size of which depends on the indentation load.

Cracks generally originate from stress concentrations. Some of the common sources of stress concentrations are contact stresses, thermal expansion mismatch, thermal

expansion anisotropy, elastic property mismatch and interfaces. Stress free cracks and cracks formed by residual stresses respond differently to the loading conditions, and affect the properties differently. Detailed fracture mechanics analysis for both types of failure exist, and have been confirmed by extensive experimentation in a number of ceramics[16-18]. Even then the micro-mechanics of failure from sub-threshold flaws is not at all well-understood, because the very nature of flaws and the stresses acting on them are not well known.

Hillig[19] has recently reviewed the important factors involved in the choice of materials for high temperature composites. Melting point is the obvious ultimate limitation, but in addition, factors like phase changes, structural changes and environmental attack need to be taken into account. This is essential, because these factors affect the melting point of the material. On the basis of melting point alone, Hillig identifyed about 200 compounds with melting points above 2000^{o}C, all of which are potential components of ceramic composites, of the present and the future.

In case of ceramic matrix composites, the reinforcing phase must be of superior strength and/or refractoriness, otherwise no property advantage would follow. It is important for the fiber to have good ductility, because the fiber is the sole contributor to improved strain at failure, the matrix being brittle.

The interactive effects between the fibers and the matrix, play very important roles in tailoring the properties of the composite. Physical compatibility between the fiber and matrix is important. Mismatch in thermal expansion between the fiber and the matrix leads to prestressing of one or the other. The stresses in the matrix phase are of greater importance than those in the fiber phase. That is because unlike metal matrix composites, failure generally initiates in the matrix phase, rather than in the fiber. The reason for this is that the matrix is far more brittle as compared to the reinforcing fibers.

Some amount of thermal expansion mismatch between the fibers and matrix is desirable[20]. Thermal expansion mismatch leads to microcrack toughening. However excessive microcracking is undesirable and leads to a drastic drop in the strength and Youngs modulus. The best composites are those in which the difference in the coefficient of thermal expansion between the fiber and matrix is of the order of 1-2x$10^{-6}/^{o}K$ [20]. Preferably, the coefficient of thermal expansion of the fibers should be greater than that of the matrix, so that the matrix is in a state of compression after composite fabrication.

The chemical compatibility between the two components, namely the fibers and matrix, also need to be taken into account. The inherent stability of the two components is difficult to predict. For example, in the alumina/zirconia

system, which is a simple eutectic type of system with very limited solubilty of alumina in zirconia and vice versa, one can expect good stability between the two components. However in a system such as the alumina/magnesia , there is the formation of an intermediate compound $MgO.Al_2O_3$. Hence in this system stability of the component phases would not be expected. Some information regarding the chemical compatibility of the phases can be obtained through thermochemical data. However, a combined theoretical and experimental approach should be carried out. In many cases, specific coatings are provided on the fibers to prevent or reduce the chemical interactions between the fiber and the matrix. As an example, boron nitride coated silicon carbide fibers have been found to be very effective in inhibiting the volatalization of the fiber surfaces. Extensive research is being pursued in the field of fiber coatings[21,22].

In addition to the physical and chemical compatibility between the two components, another important factor which needs to be accounted for is the bonding between the two components. The fiber-matrix shear properties are crucial in determining the mechanical behaviour of the composites. In a composite system in which both the components exhibit similar physical and chemical properties, the matrix tends to bond very strongly to the fibers. It has been well recognized that strongly bonded interfaces can result in fracture right through the fibers. Rice et al.[21] and

Bender et al.[22] have shown that coatings which decrease the interface bonding, lead to an increase in the strength and toughness of the composites. Marshall and Evans[23] during their studies with silicon carbide fiber reinforced glass ceramics, which exhibit outstanding properties, observed that the interface was weakly bonded. Observations of an amorphous carbon film at the interface confirmed their findings. On the other extreme, too weak an interface may result in lower strengths. Hence it is important that the interface has just the right strength. The interface should neither be too weak, nor should it be too strong. Some of the mechanisms of toughening, such as crack deflection and crack branching at the interface, rely on the existence of sufficiently weak interfaces to the preferred fracture paths. These mechanisms have been accepted after extensive experimentation and detailed analyses. Hence understanding and tailoring the interface for the best compromise between strength and toughness, is an important area of research, in which coating techniques are expected to play an important role.

The reinforcement-matrix interaction determines whether the composite has good strength, toughness and the microstructural stability to maintain these characteristics at elevated temperatures. The latter requirement derives from the perception that excellent opportunities for the use of ceramic matrix composites exist in heat engines. In these applications thermal shock, thermal fatigue, high

temperature corrosion and erosion are present, which additionally degrade the strength. Characterization of the experimental materials and better models of behaviour to guide experimentation are needed to satisfy the stringent requirements for the use of ceramic composites in heat engines. The most promising of all the systems available today are the silicon carbide reinforced ceramics[24-30]. Today, single crystal silicon carbide whiskers are available from various manufacturers. These whiskers have Young's moduli of about 690 GPa and strengths in excess of about 6.9 GPa. These whiskers are upto one micrometer in diameter, and 50 micrometers long. A number of automakers including Mercedes-Benz, General Motors, Ford, Volkswagen and Nissan have incorporated Ceramic composites into their engines. General Motors is planning to make a Ceramic engine to be used on future models. A number of gas turbine manufacturers including Allison, Pratt and Whittney and General Electric are also looking into the use of Ceramic-matrix composites in turbine engines, for the new generation of jet fighters and transport aircraft.

Until recent years, not much attention was paid to the processing techniques, employed in the manufacture of the ceramic composites. However with the advent of superior characterization techniques, it has become clear, that by employing the right processing techniques, superior mechanical and thermal properties can be achieved. This results from of better fiber-matrix distributions,

microstructures and interfacial properties.

The main requirements of the processing technique is that it should be easy to carry out, should be cost effective and should not lead to any kind of deterioration in the properties of either the fiber or the matrix. Degradation and loss of strength usually arises from mechanical damage during processing, grain growth or chemical reactions which occur especially at elevated temperatures. Ceramic composites need to be sintered at elevated temperatures to cause sufficient binding between the individual grains of the powder compact. Hot pressing is commonly employed in the manufacture of a large number of ceramic composites. In hot pressing, temperature and pressure are applied simultaneously, during the sintering of the powder compact. Although the high temperature does not have any deletrious effect on the matrix, the fibers are usually affected. Graphite fibers are most seriously affected by the oxidation occuring at elevated temperatures, and exhibit a drastic drop in strength. Silicon carbide fibers also oxidize at elevated temperatures, and loose their strength.

In recent years, new processing techniques have been developed for processing ceramic matrix composites[31-33]. The conventionally used hot pressing and slurry infiltration techniques are being replaced by the sol-gel and pyrolysis techniques. These techniques have the advantages of greater compositional homogenity, greater ease of forming and most

important of all, processing temperatures lower by hundreds of degrees Celsius, as compared to the conventional processing techniques. For covalent ceramics in particular, pyrolysis of polymeric precursors offers the potential for greatly reduced processing temperatures compared to solid state reactions, with a greater yield than the chemical vapour deposition technique. Examples include, but are not limited to, precursors to silicon carbide and silicon nitride. The sol-gel technique, although still in its developmental stage, is promising in the fabrication of ultra high purity ceramics[31-33].

The principal disadvantage of both techniques however, are the high shrinkage and low yield as compared with the conventional techniques. Lannutti and Clark[34] showed that dispersion of fibers or whiskers in a sol prevented microscopic cracking. However, shrinkage stresses lead to local porosity and microcracking on drying. Repeated impregnations are necessary to build up a sufficiently dense product. As a result, the most succesfull use to date of the sol-gel technique in ceramic composites, has been a modification of the slurry infiltration technique, with subsequent hot-pressing for densification. In spite of all these modifications, the processing costs for these processes still remains high.

Another approach to eliminate high processing temperatures, is by means of materials selection; by using systems which have low softening points. Glass matrices

have lower softening temperatures as compared to crystalline ceramics. But there is a trade-off in the ultimate high temperature strength associated with the softening of the matrix at elevated temperatures. Glass-ceramics on the other hand have lower softening points, in the glassy state in which they are fabricated. By suitable heat treatment, they can be converted to an almost 100% crystalline structure. The resulting crystalline phase has a softening point much higher than that of the glass from which it was derived. Thus it has better high temperature capabilites, in addition to being almost 100% dense, unlike crystalline ceramics which usually contain some porosity(of the order of 10%). Appropriate selection of the glass system, can result in a glass-ceramic during the fabrication process itself, without requiring any additional heat treatment to crystallize the matrix.

A large number of glass-ceramic composites have been developed with exceptionally high strength and toughness[24-28]. The fibers used include boron, silicon carbide, graphite, alumina and silicon nitride. Some of the commonly used glass-ceramic matrices include compositions in the Lithium-alumino-silicate and Magnesia-alumino-silicate systems. Single crystal whiskers of silicon carbide have been incorporated into several alumino-silicate glass-ceramic systems, with resulting strengths of about 400 MPa, Youngs modulus of about 200 GPa and fracture toughness values as high as 5-7 $MPam^{1/2}$.

Metallic glasses:

The process of rapidly cooling moulten metal has been known and studied for quite some time now. It is well known that rapidly cooling a metal refines the grain size, prevents seggregation of the constituents and improves the mechanical properties. In the late nineteen sixties, a new class of materials evolved. Chen and Turnbull[35] were the first to observe and study this new class of materials. This class of materials studied by them was obtained by rapidly cooling a palladium-silicon alloy. They observed that the structure of these "rapidly cooled melts" was very similar to that of ceramic glasses, and hence the class of metallic materials were christened as "metallic glasses".

Metallic glasses are an unique class of materials. Metallic glasses are produced by rapidly cooling molten metal at rates of the order of 10^6-10^7 ^oK/sec. The melts are usually alloys of iron, nickel, molybdenum or chromium, with alloying elements like carbon, boron, phosphorous and silicon. Metglasses possess exceptional magnetic and electrical properties[36]. They have a higher electrical resistivity as compared with conventional crystalline electric steels. They also have a higher magnetic saturation induction, coupled with a low core loss. The nickel-iron based metglass alloys have a high magnetic permeability, lower coercive field and a low

magnetorestriction. In fact, one of the major applications of metglasses, is in transformer cores. The Engineers at General Electric have envisaged that if all the distribution transformers now in service in the United States were to be replaced by amorphous metal transformers, the power saving would amount to 2000 MW a year, or about 20,000,000 barrels of cooling oil a year[36]. This saving is due to reduction in the core losses by about 70%. Other applications include stators of electrical motors. Metglass stator motors are not only much smaller in size, but are also far more efficient as compared to conventional stator motors.

Metglasses also possess exceptional mechanical properties[37]. Their fracture strength and hardness exceed that of heavily cold worked steel wires. At the same time they exhibit high fracture strains. They also have superior corrosion resistance compared to their metallic counterparts. The total plastic strain can be sufficiently large; for example 5% in compression or 100% in bending. Similarly, very large reductions can be obtained on metglasses, without any work hardening. Detailed studies on the strength and ductility of metallic glasses was made by Davis[38], and Masumoto[39] .

Structurally, metglasses are a subgroup of the amorphous metals, which also include materials produced by vapor deposition, sputtering, electrodeposition or ion bombardment. A material is termed amorphous if its atomic arrangement has no long-range translational symmetry.

Metglasses do not possess any long-range symmetry. However, they do posses a high degree of short-range structural order, due to the topological and chemical constraints imposed by the local close packing of the atoms. The study of metglasses has shown them to be the low temperature continuation of the liquid phase, with a structure that is fundamentally distinct from any crystalline phase, and to a large extent independant of the method of preparation.

Ceramic composites studied so far have either incorporated metallic or ceramic reinforcements. Until a few years back, metallic glasses were never considered as reinforcements for composite systems. In 1977, metglasses were used for the first time to reinforce polymer matrices. Hornbogen et al.[40-42] demonstrated that even a very small volume fraction of metglass could dramatically improve the strength and toughness of brittle polymer matrices. The transverse strength of unidirectional composites is usually very low, owing to the high degree of anisotropy present in them. However unidirectionally reinforced metglass-polymer matrix composites, have shown to have transverse strengths almost 50% of their longitudional values, and transverse Young's moduli of almost 90% of their longitudional values. On the other hand, conventional graphite-epoxy composites have transverse strengths and Young's moduli only about 10% of their longitudional values.

Metallic glass reinforcements are usually obtained in the form of thin ribbons, which are usually 40-100

micrometers thick. The high surface area provides for a very good bonding with the matrix. Metglass ribbons are available commercially, and are marketed by Allied Chemical Corp. The currently available metglasses include alloys of iron and nickel, in combination with other elements like chromium, cobalt, molybdenum, carbon and silicon.

The main disadvantage of these metglass alloys, is their low recrystallization temperatures. Metallic glasses are not only thermodynamically metastable with respect to their corresponding crystyalline phases, but are also unstable with respect to their relaxed glassy states. Although the metglasses crystallize only when heated above the recrystallization temperature, they do undergo structural relaxation at lower temperatures. These two processes lead to slight loss in ductility. Although the mechanism of the process is not clear, it has been proposed that the loss of ductility may be as a consequence of clustering of metalloid atoms. Chen [43] suggested that the loss of ductility may be as a result of very fine scale phase seperation. It has also been observed that stability is greatest in alloys with the fewest costituents. Hence it has been concluded that the decrease in the fracture strain of metglasses on heating, is a result of the change in the nature of the bonding between constituent atoms.

Some metglass alloys with very high strengths and recrystallization temperatures upto 1200^{o}C have been produced[43], although their processing has been very

difficult. These metglasses provide an unique basis for developing metglass reinforced glass, or glass-ceramic composites, for high temperature applications.

The main objectives of the present investigation were:

1. To study the feasibility of using metglass ribbon reinforcements in the development of ceramic-matrix composites, which have a good potential for high temperature applications.
2. To study the mechanical properties such as fracture strength and Young's modulus, of both the unreinforced matrix material and the composite having only a small volume fraction of metglass ribbon reinforcement, in order to understand the strengthening effects due to the high strength reinforcements.
3. To study the effects of increasing volume fraction of metglass ribbon reinforcement, on the mechanical properties of the composite.
4. To study the interactive effects such as interfacial bonding and thermal expansion mismatch between the metglass ribbons and the matrix, and to corelate them with properties such as fracture toughness.
5. To understand the reasons for the observed behaviour of the composite, based on fractographic studies.

EXPERIMENTAL PROCEDURES

Specimen Preparation:

The metglasses used in the present study were obtained from Metglas Corporation, a subsidiary of Allied Chemical Company. The company manufactures metglasses of different compositions on a commercial basis. Two different metglasses were used in the present study; one a Nickel-based metglass(MBF-75), and the other an Iron-based metglass(MT 2605/S-2). The compositions and properties of both metglasses are listed in Table 1. Both metglasses have recrystallization temperatures in the range of 550^{o}C.

Initial studies on the composite fabrication were carried out using borosilicate slide glass and Corning Glass Code 0080. Various processing techniques including hot-pressing were tried out. However, these techniques were found to be unsuitable for the current system, which incorporated metglasses having recrystallization temperatures of the order of 550^{o}C. Both, the borosilicate slide glass and Corning Glass Code 0080, had softening temperatures well above 600^{o}C. Sol-gel technique was also found to be unsuitable, due to the high softening temperature of the nearly pure silica powder. It was also difficult to incorporate the metglass ribbon reinforcement into the gel.

TABLE 1. Properties of the Metglass ribbons reinforcements:

Property	Metglas MT 2605/S-2	Metglas MBF-75
Chemical composition :	Fe : 78% B : 13% Si : 9%	Ni : 50% Co : 23% Cr : 10% Mo : 7% Fe : 5% B : 5%
Crystallization temp. :	550^{o}C	605^{o}C
Elastic modulus :	85 GPa	70 GPa
Yield strength :	> 700 MPa	*
Coefficient of thermal expansion :	76 x 10^{-7}/ ^{o}C	*
Density :	7.18 g/cc	*

* not specifyed by manufacturer

Based on the initial experimentation, Corning Glasses Code 7572 and 8463 were selected as the matrix materials for the present investigation. These two glasses are lead-borosilicate-aluminate glasses, containing high percentages of zinc oxide. The compositions and properties of both the glasses are listed in Table 2. Both the glasses, 7572 and 8463, have softening temperatures in the range of 400°C. These glasses crystallize during the sintering process itself, resulting in a glass-ceramic, which will not exhibit softening as the parent glass. These glass-ceramics are stable upto their melting temperature.

The wet-pressing technique was used in making the specimens. The glass powder was mixed with 3% amyl acetate binder. The powder was then compacted in a steel die, under a pressure of 3000 psi, using a Tinus-Olsen machine. After holding the pressure on the specimen in the die for a period of 5 minutes, the pressure was released and the specimens were removed from the die.

The specimens were then placed on a firebrick covered with a thin foil of copper or aluminum, to prevent the specimens from sticking to the brick surface. The specimens were then placed in an electrical resistance furnace for sintering. The specimens were heated to 200°C, in the furnace set at that temperature, for a total period of 20 minutes. This was carried out in order to allow the binder to evaporate. The furnace temperature was then raised in steps of 20°C, upto the sintering temperature of 400°C. The

TABLE 2. Properties of the matrix glasses:

Property	Corning Glass 7572	Corning Glass 8463
Softening point :	375°C	370°C
Coefficient of thermal expansion :	95 x 10^{-7}/ °C	105 x 10^{-7}/ °C
Density (powder) :	3.8 g/cc	3.8 g/cc
(fired) :	6.0 g/cc	6.2 g/cc
Continuous service temperature :	450°C	450°C
Chemical composition :	PbO : 70%	PbO : 84%
	B_2O_3 : 5-10%	B_2O_3 : 5-10%
	SiO_2 : 2-5%	SiO_2 : 2-5%
	Al_2O_3 : 1-5%	Al_2O_3 : 1-5%
	ZnO : 10-20%	ZnO : 10-20%

specimens were sintered in the furnace at this temperature for a period of 90-120 minutes. Once the sintering was completed, the furnace temperature was raised to 450°C, and the specimens were crystallized at this temperature. After holding for about 20 minutes at 450°C, the furnace was shut off, and the specimens were furnace cooled down to room temperature.

Measurement of the Elastic properties:

The non-destructive Dynamic Resonance technique[44] was used to characterize the the elastic properties of the specimens. The technique is based on the standing wave phenomenon. When a specimen undergoes longitudional or torsional vibration, its length contains an integral number of half wavelengths. The amplitude of vibration of the specimen will reach a maximum value at a particular frequency, called the resonance frequency. The Youngs modulus of the specimen is proportional to the square of the flexural resonant frequency, while the shear modulus is proportional to the square of the torsional resonant frequency.

Hence, $\ell = nw/2$; $v=wf=2\ell f/n$

where, ℓ is the length of the specimen

n is an integer

w is the wavelength, and

f is the resonant frequency.

The measuring system consists of a driving circuit, a pick-up circuit and a specimen support. A schematic diagram of the set-up is shown in the Figure 1. A variable frequency synthesizer/function generator(Hewlett-Packard 3325A) served as the signal source. The sinusoidal electrical signal was converted into mechanical vibrations via a high power piezoelectric trasducer(model 62-1, Astatic Corp. Ohio). The mechanical vibrations were passed through a support thread to the specimen. The specimen arrangement is shown in Figure 2. The vibrations were then picked up by another support thread, and were fed to the pick-up transducer. The mechanical vibrations which were picked up were converted into an electrical signal, which was amplified and filtered(by a 4302 dual 24db octave filter amplifier , by Ithaco). The amplified and filtered signal was fed to an oscilloscope(V-100 100MHz oscilloscope by Hitachi) and voltmeter(8050-A digital by Fluke), which were connected in parallel.

To calculate the Young's modulus, it is necessary to know the type and mode of vibration. A prismatic bar can be excited in a variety of vibrational modes, which includes the fundamental frequencies of the flexural and torsional modes, and their overtones. The vibrational mode can be identifyed by locating the position of the vibrational nodes and antinodes, along the specimen length, in which a standing wave vibration forms. The position of the nodal and

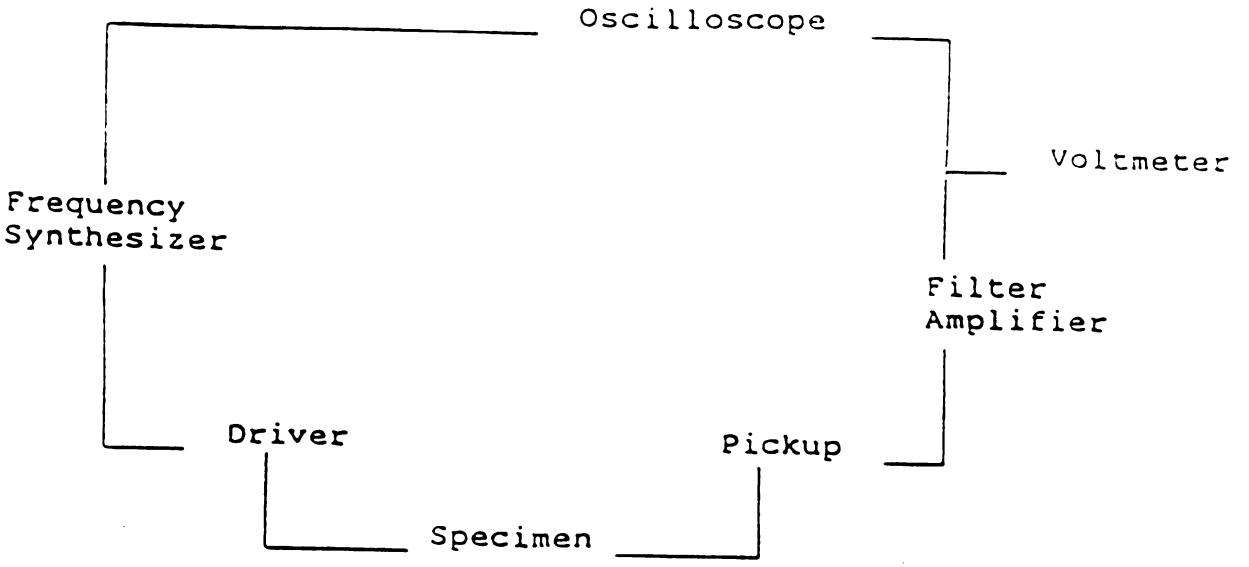

FIGURE 1. **Experimental setup for the Dynamic Resonance test.**

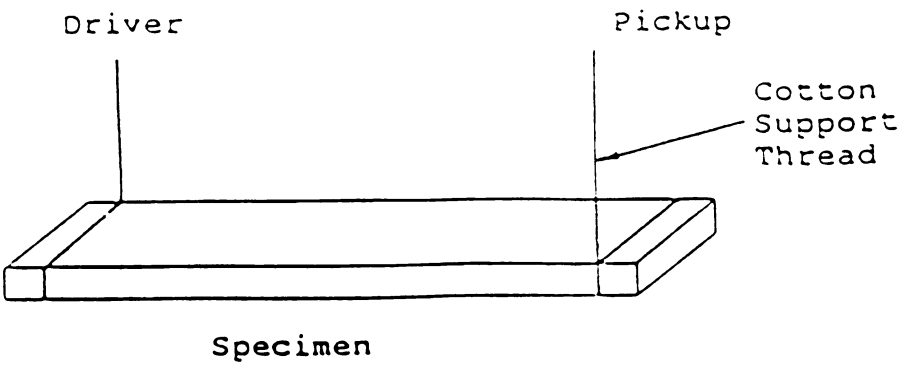

FIGURE 2. Specimen configuration in the Dynamic Resonance test.

antinodal points can be determined by mechanically probing the bar. In this study the nodal and antinodal positions were probed using a sewing needle. When the needle is set at a nodal point, the amplitude of the signal changes very little. If the needle is positioned away from the node, the needle tends to dampen the mechanical vibrations, and the amplitude of vibration is reduced. The position of the nodes for the various modes of vibration, in terms of fractions of the length of the specimen, are presented in Table 3.

The resonant frequency is characteristic of the specimen, and depends on factors like porosity of the specimen, microstructure and residual stresses.

The Young's modulus(E) can be determined from the flexural vibration mode using the following formula:

$$E = (6.2824 f^2 \ell / km^2) \varsigma t$$

where, E is the Youngs modulus of the sample
f is the flexural resonant frequency
ℓ is the length of the specimen
k is the radius of gyration
m is a constant depending on the mode vibration, and is equal to 4.73 for the fundamental mode.
ς is the density of the specimen, and
t is the shape factor.

TABLE 3. Position of the nodes for various modes of vibration, in terms of fractions of the specimen length[44]:

Mode of vibration	Flexural vibration	Torsional vibration
Fundamental	0.224 0.776	0.5
First overtone	0.132 0.500 0.868	0.25 0.75

The shape factor is approximated by the equation:

$$t=1+6.58(1+.0752+.8109\nu^2)(d/b)^2-.868(d/b)^4-8.34(1+.2+2.17\nu^2)(d/b)^4$$
$$1-6.34(1+.14+1.53\nu^2)(d/b)^2$$

where, b is the width of the specimen
d is the specimen thickness, and
ν is the Poisson's ratio of the specimen.

Similarly the shear modulus(G) can be determined from the torsional resonant frequency, using the following formula:

$$G = 4\rho R\ell^2 f^2/n^2$$

where, G is the shear modulus of the specimen
ρ is the density of the specimen
ℓ is the length of the specimen
f is the torsional resonant frequency
n is an integer, and is 1 for the fundamental mode, and
R is the shape factor.

The shape factor(R) is approximated by the equation:

$$R = (1+(b/a)^2)/(4-2.5(a/b)(1-2/(e^{b/a}+1))(1+(0.0085a^2b^2/\ell^2))$$

where, a is the specimen thickness

b is the width of the specimen, and

ℓ is the length of the specimen.

The Poisson's ratio(ν) for the specimen can be determined from the Young's and shear moduli of the specimen, by using the formula:

$$\nu = (E/2G)-1.$$

Similarly, the bulk modulus(K) can be determined by using the formula:

$$K = (EG)/3(3G-E).$$

A program developed by Case[45] was used for calculating the various elastic constants of the specimens. The program uses the shape factor calculated for a Poisson's ratio of 0.25, which is about the same as that for the glass-ceramic system being investigated. The system under investigation has a Poisson's ratio in the range of 0.23 to 0.28.

During the study of the selected composite system, the flexural resonant frequency was readily detected. However the torsional resonant frequencies of the specimens could

not be detected. The shear modulus of the specimens were calculated by using the values of the Young's modulus, and by using a poissons ratio of 0.25.

Strength Measurements:

The measurement of strength by the bend test is the basic procedure adopted in testing ceramics and ceramic matrix composites. The bend test is commonly used for brittle ceramic materials, as compared to the tensile test, because it does not require grips and hence is less complicated to perform.

The three point bend test was used for measuring the fracture strength of the specimens[46]. The Modulus of Rupture(MOR), is defined as the fracture strength of a material under a bending load. For the three point bend test, using rectangular bar shaped specimens, the Modulus of Rupture is given by the formula:

$$MOR = (3PL)/(2bd^2)$$

where, P is the load at fracture
L is the span of loading
b is the width of the specimen, and
d is the specimen thickness.

The A.S.T.M. specifications C-158 and C-203/85 require that:

1. The loading rate should be between 8000 and 12000 psi/min.
2. The span to thickness ratio be between 2 and 20. i.e. 20>(L/d)>2; recommended (L/d)=16.
3. The span to width ratio be greater than 0.8. i.e. (L/b)>0.8; recommended (L/b)=4
4. The width to thickness ratio be greater than 1. i.e. (b/d)>1; recommended (b/d)=4.

The three point bend tests were carried out with an Instron machine, using a crosshead speed of 0.05cm/min, and a chart recorder speed of 1cm/min. The span of the three point bending fixture was varied depending upon the dimensions of the specimen, and in accordance with A.S.T.M. specification C-203/85. Although the dimensions of the specimens varied, the dimensions of the metglass ribbon reinforcements used in all the specimens remained the same. The width of the metglass ribbons used was 0.5 cm, and the thickness was 45 micrometers. The fractured surfaces of the specimens were also observed using a Scanning electron microscope. A Hitachi model S-415/A scanning microscope was used for the purpose. Since the specimens being observed were electrically non-conductive, their surfaces had to be coated, in order to prevent a charge bulid-up on their surfaces. The specimen surfaces were coated with gold, using a sputtering unit. Argon gas was back charged into the vacuum chamber during the coating process.

Thermal shock resistance testing:

One of the important properties of ceramics which makes them very attractive in a number of applications, is their resistance to high temperatures. Ceramics retain their strengths upto relatively higher temperatures as compared to metals. However a majority of applications demand that the components be cyclically heated and cooled down, to the operating temperatures and room temperatures respectively. This results in the thermal shocking of the specimens. Large thermal stresses are generated due to thermal shocking, and these thermal stresses relieve themselves by cracking the specimen. This is more pronounced in case of ceramics, because of the absence of plastic deformation, as in case of metals.

Cracking is detrimental to the properties of the ceramic, and leads to a reduction in the strength and elastic modulus. In extreme cases it could even lead to failure. Hence a study of the thermal shock resistance is important in characterizing the high temperature capabilities of the ceramic.

Tests to evaluate the thermal shock resistance, both for the matrix and composite specimens, were carried out using procedures described in literature [47-49]. Rectangular bar shaped specimens were used for the matrix and reinforced composites. The surfaces of the specimens

were ground to a 600 paper finish. The specimens were then heated in a resistance furnace and soaked at the set temperature for a total period of one hour. After soaking, the specimens were quenched in water, at a temperature of 42^{o}C. The specimens were allowed to cool for a period of 10-15 minutes, and were then removed from the cooling media for testing.

The three point bend test was performed on the thermally shocked specimens, using an Instron machine with a cross head speed of 0.05cm/min. The change in the Modulus of Rupture with increasing thermal shock was measured. The Young's modulus was also measured using the Dynamic Resonance technique.

Other details of the test are as follows:

Specimens: 7572 Leaded glass matrix specimens and
Metglass 2605/S-2 reinforced 7572
specimens.(Volume fraction = 0.8%)

Water temperature: 42^{o}.

Furnace temperatures: 1)200^{o}C 2)250^{o}C 3)300^{o}C 4)400^{o}C
5)450^{o}C.

Temperature delta T's 1)158^{o}C 2)208^{o}C 3)258^{o}C 4)358^{o}C
5)408^{o}C.

The fractured surfaces of the specimens were also observed under a scanning electron microscope.

Fracture toughness measurements:

The fracture toughness of the specimens was measured using two techniques; the Notched Beam technique[50] and the non-destructive Indentation technique[13-14].

The Notched Beam technique is very widely used for measuring the toughness of a wide variety of materials, and also for a range of specimen geometries. The most simple and commonly used one is the single edge notched beam specimen, loaded in bending, as shown in the Figure 3. Either three or four point bending can be used for loading the specimen. Uniform tension loading can also be used, but is less satisfactory owing to the difficulties in gripping and alignment.

For the three point bend geometry, K_{IC} can be calculated from the following form of the Griffith relation:

$$K_{IC} = (6\, Ma^{1/2}/bw^2)Y$$

where, K_{IC} is the fracture toughness

σ is the fracture stress

a is the crack depth

b is the specimen thickness

w is the specimen width

M is the applied bending moment at fracture and is equal to Ps/4

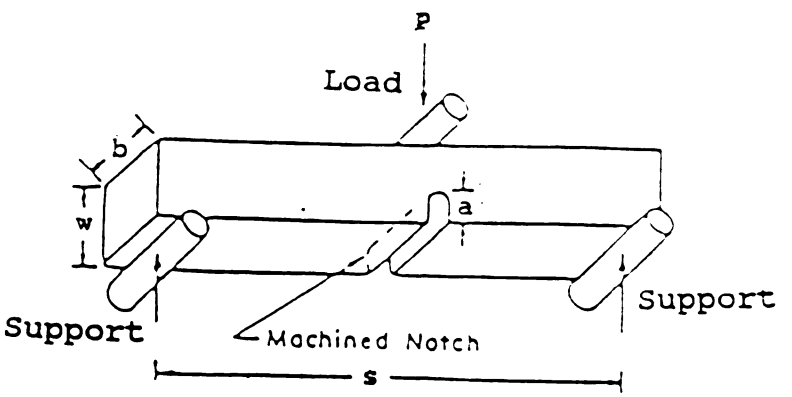

FIGURE 3. Experimental setup for the Single Edge Notched Beam test.

where, P is the load at failure

and s is the span of loading.

Y is a dimensionless parameter which depends on the ratio a/w and the type of loading as,

$$Y = A_o + A_1(a/w) + A_2(a/w)^2 + A_3(a/w)^3 + A_4(a/w)^4$$

where, A_o, A_1, A_2, A_3 and A_4 are constants

a is the crack depth, and

w is the width of the specimen.

The constants (A_0, A_1, A_2, A_3 and A_4) have values as given in Table 4. The variation in the shape factor(Y), with the ratio of the crack depth to the specimen thickness(a/w), is illustrated in Figure 4.

The equation for the fracture toughness assumes that the artifically induced crack, which becomes unstable, has zero width, extends to the full breadth of the specimen, and that its depth is uniform and is precisely known. The notch in the specimens to be tested, were saw cut using a diamond blade, on an Isomet cutting machine. Since saw cutting the notch can introduce a cracked zone at the notch root, which acts as a deliberately introduced precrack, steps need to be taken to minimize the effect of these cracks. It has been seen that annealing the specimens is beneficial in reducing the effect of these cracks[50]. The

TABLE 4. Values of the coefficients A_o, A_1, A_2, A_3 and A_4 for different bending configurations[44]:

Type of bending	A_o	A_1	A_2	A_3	A_4
Three point:					
1. s/w=8	+1.96	-2.75	+13.66	-23.98	+25.22
2. s/w=4	+1.93	-3.07	+14.53	-25.11	+25.80
Four point:	+1.99	-2.47	+12.97	-23.17	+24.80

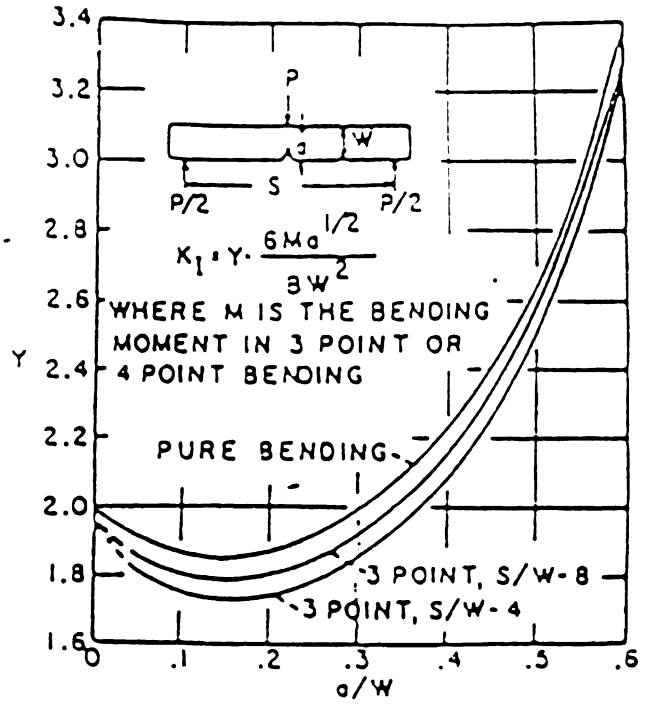

FIGURE 4. Variation in the shape factor(Y) with the ratio of crack depth(a) to specimen thickness(w) [46].

specimens were annealed in a furnace at 200^{o}C for a period of 2 hours. The specimens were furnace cooled, down to room temperature. The specimens were then tested in three point bending, using an Instron machine with a cross head speed of 0.05cm/min.

Fracture toughness by the Indentation technique:

The Vickers microhardness indentation, at loads high enough to produce a half penny surface crack, has become a widely used technique for assessing the fracture toughness of ceramics[13-14]. The various parameters associated with an indentation obtained on loading with a Vickers diamond indentor are illustrated in Figure 5. According to the theory, the radius of the half penny crack c, bears a characteristic relation to the indentation load P as,

$$c=kP^{2/3}.$$

Lawn et al.[13] presented a detailed fracture mechanics analysis for assessing the fracture toughness, according to which,

$$K_{IC} = d(E/H)^{0.5}(P/c^{1.5})$$

where, K_{IC} is the fracture toughness

H is the hardness of the specimen

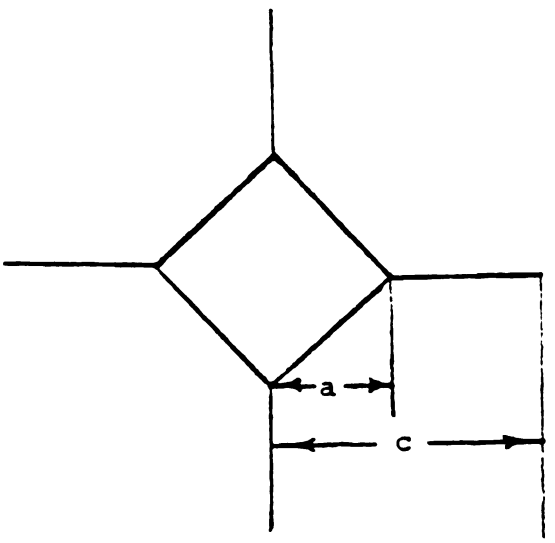

FIGURE 5. Length of the crack(c) and semi-diagonal(a) of a Vicker's indentation.

E is the Youngs modulus of the specimen

P is the indentation load

c is the crack length, and

d is some dimensionless constant.

The constant d, is primarily a function of the geometry of the indentor. The value of d has been established by calibration with the known fracture toughness values of a number of ceramics. The value of d for the Vickers indentor is 0.014.

The indentation technique was only useful in obtaining the toughness values for the unreinforced specimens. The specimens were mounted in Lucite, and the surface of the specimens were wheel polished to give a smooth finish. The specimens were indented using a Beuhler microhardness tester. Following are the details of the experiment:

Load : 0.3Kg

Loading time : 20 secs

Loading speed : 50 micrometers/sec.

Three specimens were tested by this method, and a total of 25 indentations were made on each specimen.

Interfacial bond strength measurement:

Some of the important interactions between the failure processes and material paramaters in composites, can be understood by considering the mode of crack propagation in the composite. For a crack subjected to an uniaxial tensile stress normal to the plane of the crack, the presence of the crack results in additional tensile stresses parallel to the plane of the crack.

From the accompanying Figure 6, it can be seen that when a crack in the matrix meets a fiber, the stresses at the tip would tend to cause fiber failure, while the stresses perpendicular to the tip will lead to tensile seperation at the interface. The processes which occur depend upon the values of the critical stresses for these processes.

For a strongly bonded system, the ratio of the tensile stress to the shear stress is small, and the amount of debonding is small. On the other hand, a larger ratio of the tensile to the shear stresses indicates a weaker bond and higher degree of pull-out.

A weaker bond between the fiber and matrix is preferred over a very strong bond. If the interfacial bond is very strong, the propagating crack does not "see" the fiber, and the composite fails in a manner similar to that of the matrix. It is essential that some slip occurs between the fiber and matrix.

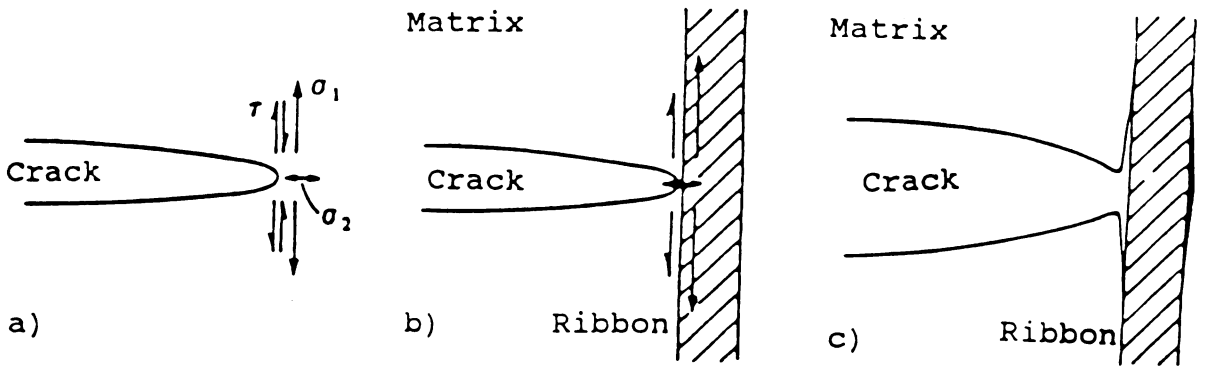

FIGURE 6. a) Schematic representation of the stresses acting at the crack tip.
b) Crack tip at the ribbon interface.
c) Interface splitting and crack opening when the crack intersects the ribbon [51].

The pull-out test[51] was carried out in order to evaluate the interfacial bond strength. A schematic of the experimental setup used is illustrated in Figure 7. The metglass ribbons were cut from the foil such that the length of each ribbon was 3.45cm and the width was 0.5cm. The ribbons had a thickness of 45 micrometers. For the special geometry of the metglass ribbons, the tensile stress required to produce bond breakage is determined by balancing the tensile and shear stresses. Hence,

$$\sigma\, bd = 2(b+d)\, T\, \ell_e$$

where T is the interfacial shear strength

σ is the tensile stress for pullout

ℓ_e is the embedded length of the ribbon

b is the width of the fiber, and

d is the fiber thickness.

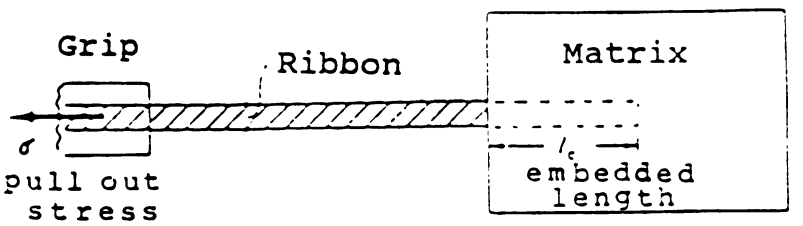

FIGURE 7. Experimental setup for the pullout test.

RESULTS AND DISCUSSION

Elastic properties:

The results of the experimentally measured elastic constants for various metglass and matrix combinations are presented in Table 5.

It is clearly evident that with even a low volume fraction of 0.75% of metglass reinforcements, an increase in the Young's modulus of the order of 25% can be obtained. Such a marked increase was also noted by Hornbogen et al.[40-42] in their studies on the metglass reinforcement of polymer matrices. They noted an increase of almost 100% in the Young's modulus for an epoxy matrix reinforced with a 1-2% volume percent of Metglass 2826 reinforcements.

In the present studies the Metglass 2605/S-2 reinforced 7572 matrix exhibited the maximum increase in the elastic properties. The MBF-75 reinforced 7572 matrix was next best. Although the 8463 matrix composite did show a significant increase in the elastic properties as compared to the matrix alone, the values of the elastic constants were significantly lower than those of the 7572 matrix

TABLE 5. *Elastic* Properties of the Matrix and Composite:

Ceramic Glass Matrix	Metglass Reinforcement	Volume Fraction	E (GPa)	G (GPa)	K (GPa)	ν	% increase E	% increase G	% increase K
7572	-	0%	33.4	13.4	22.3	0.25	-	-	-
8463	-	0%	28.1	11.2	18.7	0.25	-	-	-
7572	MT 2605/S-2	0.73%	44.0	17.6	29.3	0.25	31.7	31.7	31.6
7572	MT 2605/S-2	1.24%	47.7	18.7	35.1	0.25	42.8	39.6	57.4
7572	MT 2605/S-2	1.64%	69.4	27.8	46.3	0.25	108	108	108
7572	MBF-75	0.74%	42.1	16.8	28.6	0.25	25.9	25.3	28.5
8463	MBF-75	0.69%	36.0	14.4	24.0	0.25	28.0	28.2	27.9
8463	MBF-75	0.73%	40.8	16.3	27.2	0.25	45.4	45.4	45.1

composites. Based on these results the 7572 matrix was chosen for further investigation. In particular, the 7572 matrix reinforced with MT 2605/S-2 ribbons, was studied in detail.

The elastic properties of specimens containing 0.73%, 1.24% and 1.64% reinforcement were measured. It was observed that the composite system did not follow the rule of mixtures. According to the rule of mixtures

$$E_c = E_m V_m + E_f V_f$$

where, E denotes the Young's modulus, V the volume fraction, and the subscripts m, f and c refer to the matrix, reinforcement and composite respectively. Table 6 compares the values of the Youngs modulus obtained experimentally, with those calculated using the rule of mixtures.

The discrepancy in the two values arises from the proven fact that the rule of mixtures holds good only when the strain in the matrix is equal to the strain in the ribbons, that is in the case of ideal cohesion. However, Hornbogen et al.[40] in their studies of metallic-glass reinforced polymer matrix composites showed that the rule of mixtures can be applied to such a system, provided the volume fraction of the reinforcement is greater than some

TABLE 6. Comparison of the experimentally measured and theoretically calculated(rule of mixtures) values of Young's modulus:

Volume fraction of reinforcement (percentage)	Theoretically calculated Young's Modulus (rule of mixtures)	Experimentally measured Young's Modulus
0.73%	33.78 GPa	44.03 GPa
1.24%	34.04 GPa	47.70 GPa
1.64%	34.24 GPa	69.43 GPa

critical value. At the critical volume fraction of reinforcement, the ribbons and matrix are assumed to carry equal load. Hence,

$$E_m V_m = E_f V_f$$

$$V_f(\text{critical}) = E_m/(E_m+E_f).$$

For the material combination used here, V_f(critical) is equal to 28.2%, which is far higher than the volume fraction of reinforcements used in the current studies.

A better understanding of the elastic properties can be obtained by considering the equations developed by Halpin and Tsai[52].

According to the Halpin-Tsai theory

$$E_c/E_m = (1+\eta\xi V_f)/(1-\eta\xi)$$

where, E_c is the composite modulus

E_m is the matrix modulus

V_f is the volume fraction of the reinforcement

η is the reinforcing efficiency, which is

equal to one for a strongly bonded system, and

ξ is an emperical constant.

The value of ξ depends on various characteristics of the reinforcing phase such as shape, aspect ratio, packing geometry etc. It is necessary to determine the value of emperically, by fitting the values of ξ to the experimental results. For the system under consideration, the best fit is obtained for a value of ξ=65.

The variation in the Young's modulus with increasing volume fraction of metglass ribbon reinforcement, is shown in Figure 8. When the reinforcement increases beyond a certain value, the increament in the Young's modulus goes up sharply. This indicates that the contribution to the composite modulus, due to the ribbons, is much greater than the contribution due to the matrix. By using higher percentages of reinforcements(of the order of 25-30%), dramatic improvements in the composite modulus can be expected.

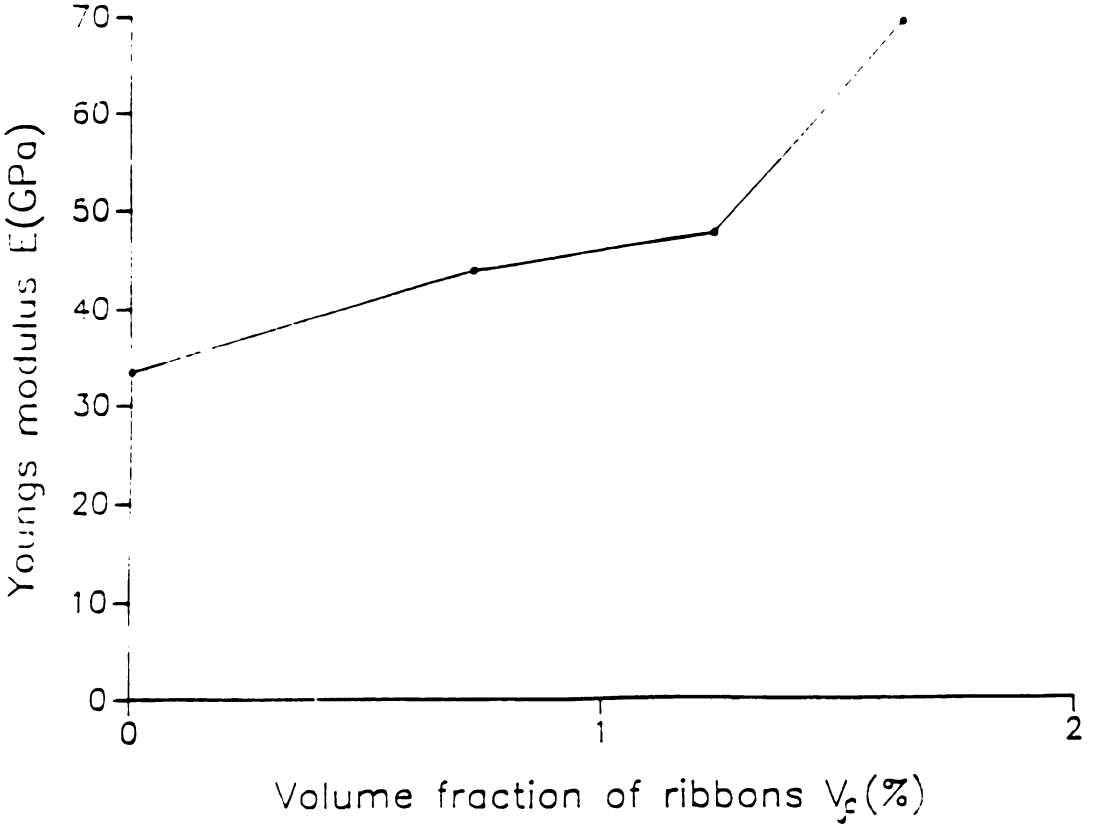

FIGURE 8. Variation in the Young's modulus of the composite with increasing volume fraction of metglass ribbon reinforcement.

Strength measurements:

The results obtained from the three point bend tests are presented in Table 7.

It can be seen from the results that the introduction of even a very small volume fraction of the metglass ribbon reinforcements leads to a significant increase in the MOR. The load versus elongation curve for the bend test, which can be envisaged from the plot given in Figure 9, shows two distinct regions of varying slopes. The initial region has a smaller slope. At some critical point during the test, the slope of the load versus elongation curve changes, and the curve becomes steeper. This behaviour remains unchanged until failure, when the load suddenly drops to zero.

In order to explain the nature of the load versus elongation curve, it is necessary to understand the mechanics of reinforcement of the system[53]. In case of the metglass/glass-ceramic system, the reinforcing metglass ribbons not only have a higher fracture strength, but also a higher fracture strain, as compared to the brittle glass-ceramic matrix. The stress versus strain curves for the ribbons, matrix and composite are illustrated in Figure 9. When the strain in the reinforcing fibers for a composite system, is greater than the strain in the matrix, two different failure sequences can be envisaged, depending on

TABLE 7. Three point bend test results:

Ceramic Glass Matrix	Metglass Reinforcement	Volume fraction	MOR (MPa)	% increase in MOR	E (GPa)
7572	-	0%	14.98	-	26.15
8463	-	0%	11.30	-	-
7572	MT 2605/S-2	0.8%	28.25	88.59	5.32*
7572	MT 2605/S-2	1.24%	30.22	101.70	-
7572	MT 2605/S-2	1.64%	41.25	175.40	-
7572	MBF-75	0.74%	32.27	115.39	-
7572	MBF-75	1.01%	33.25	121.96	-
8463	MBF-75	0.68%	20.42	80.70	-
8463	MBF-75	0.69%	21.62	91.33	-
8463	MBF-75	0.71%	22.60	100.00	-
8463	MBF-75	0.73%	23.16	104.95	-
8463	MBF-75	0.77%	25.3	124.20	-

* values which do not agree with those obtained by Dynamic Resonance.

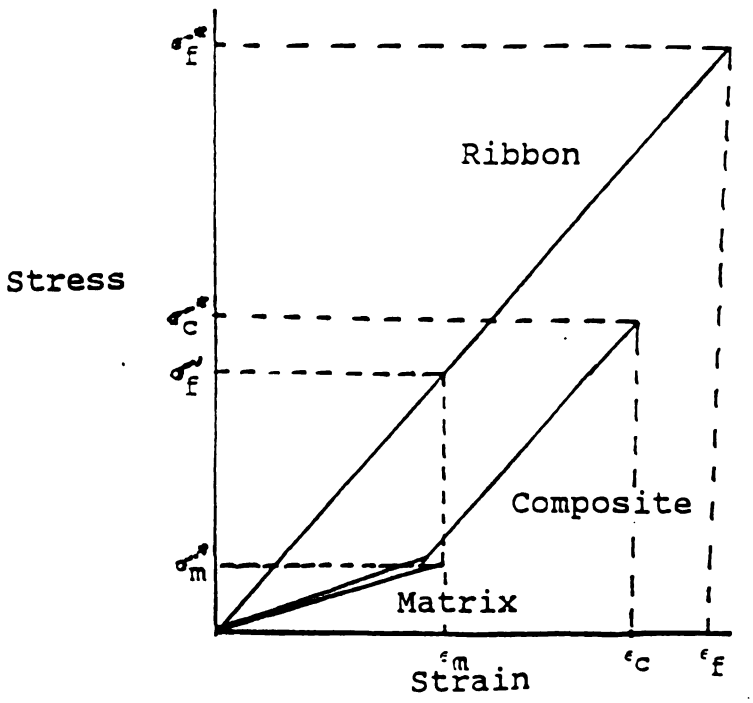

FIGURE 9. Stress-strain curves of the ribbon, matrix and composite.

the volume fraction of the reinforcing phase. For low volume fractions of reinforcements, the strength of the composite depends primarily on the strength of the matrix. The matrix fractures before the fibers, and then all the load is transferred to the fibers. When the volume fraction of the reinforcing fibers is low, the reinforcing fibers are unable to support this load and break, and thus,

$$\sigma_c^* = \sigma_f' V_f + \sigma_m^* V_m$$

where σ_c^* is the fracture stress of the composite

σ_m^* is the fracture stress of the matrix

σ_f' is the stress transferred to the fiber when the matrix cracks

V_m is the volume fraction of the matrix, and

V_f is the volume fraction of the fibers.

This is schematically illustrated in Figure 10.

When the volume fraction of the reinforcement fibers is large, the matrix takes only a small proportion of the load, because the Young's modulus of the fiber is greater than the Young's modulus of the matrix, so that when the matrix fractures, the transfer of load to the reinforcing fibers is insufficient to cause fracture. Provided it is still possible to transfer the load to the fibers, the load on the composite can be increased, until the fracture strength of the fibers is reached. Then,

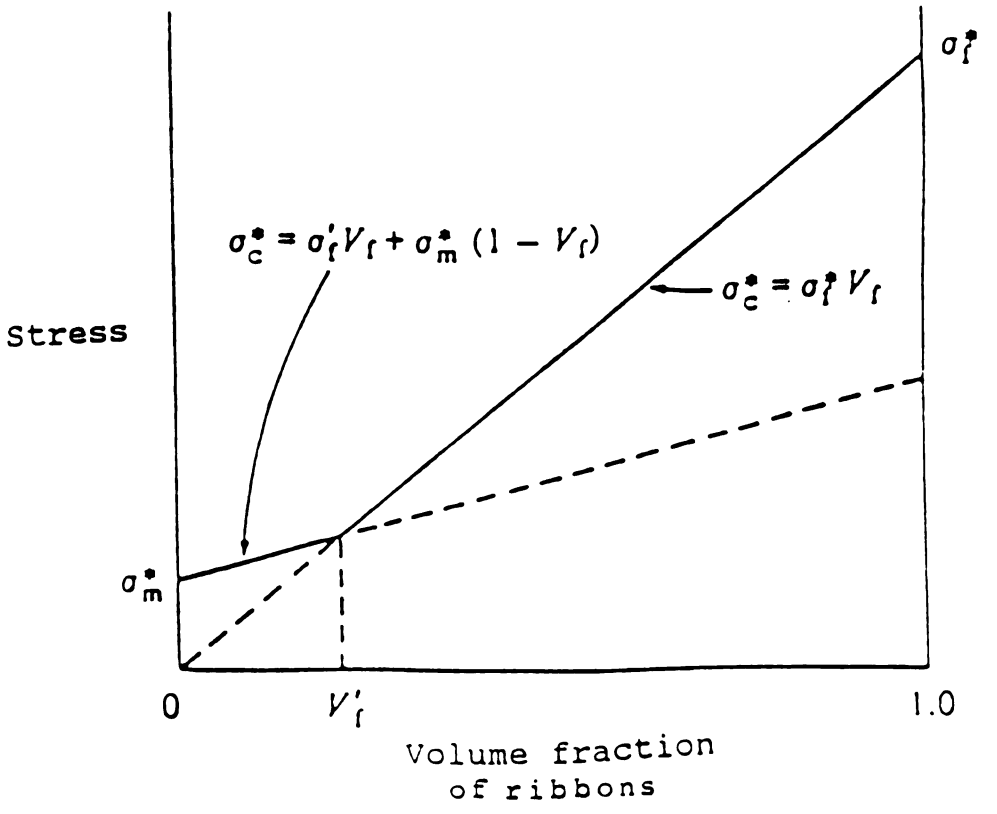

FIGURE 10. Variation in the fracture strength of the composite with increasing volume fraction of metglass ribbon reinforcement[53].

$$\sigma_c^* = \sigma_f^* V_f$$

where, σ_c^* is the fracture stress of the composite

σ_f^* is the fracture stress of the fibers, and

V_f is the volume fraction of the fibers.

The fracture strength varies with the volume fraction of the reinforcing phase. The cross over point is obtained by combining the two equations, and is given by

$$V_f = (\sigma_m^*)/(\sigma_f^* - \sigma_f' + \sigma_m^*)$$

where, V_f is the critical volume fraction

σ_m^* is the fracture stress of the matrix

σ_f^* is the fracture stress of the fibers, and

σ_f' is the stress transferred to the fibers when the matrix cracks.

During the study, the strength of various metglass/glass-ceramic systems was measured. The Metglass MT 2605/S-2 reinforced 7572 matrix gave the best results and were chosen for further studies.

For the given composite system, the crossover point

occurs at a volume fraction of 0.5% reinforcement. However the specimens tested had volume fractions of the reinforcement phase well above the critical volume fraction. This is in fact reflected in the load versus deformation curve. In the initial portion of the curve the matrix carries all the load. However once the fracture strength of the matrix is reached, the matrix fractures and the load is transferred to the reinforcing ribbon. The load corresponding to the changeover point agrees with the value obtained for the matrix phase. The variation in the Modulus of Rupture of the composite specimens, with increasing volume fraction of metglass ribbon reinforcements can be seen in Figure 11.

The Youngs modulus for the given composite system was also calculated using the formula,

$$E = (PL^3)/(48ID)$$

where, E is the Youngs modulus

P is the load at fracture

L is the span of loading

D is the deflection, and

I is the Moment of Inertia.

For rectangular bar shaped specimens, the Moment of Inertia(I) is given by,

$$I = bh^3/12$$

where, I is the Moment of Inertia

b is the width of the specimen, and

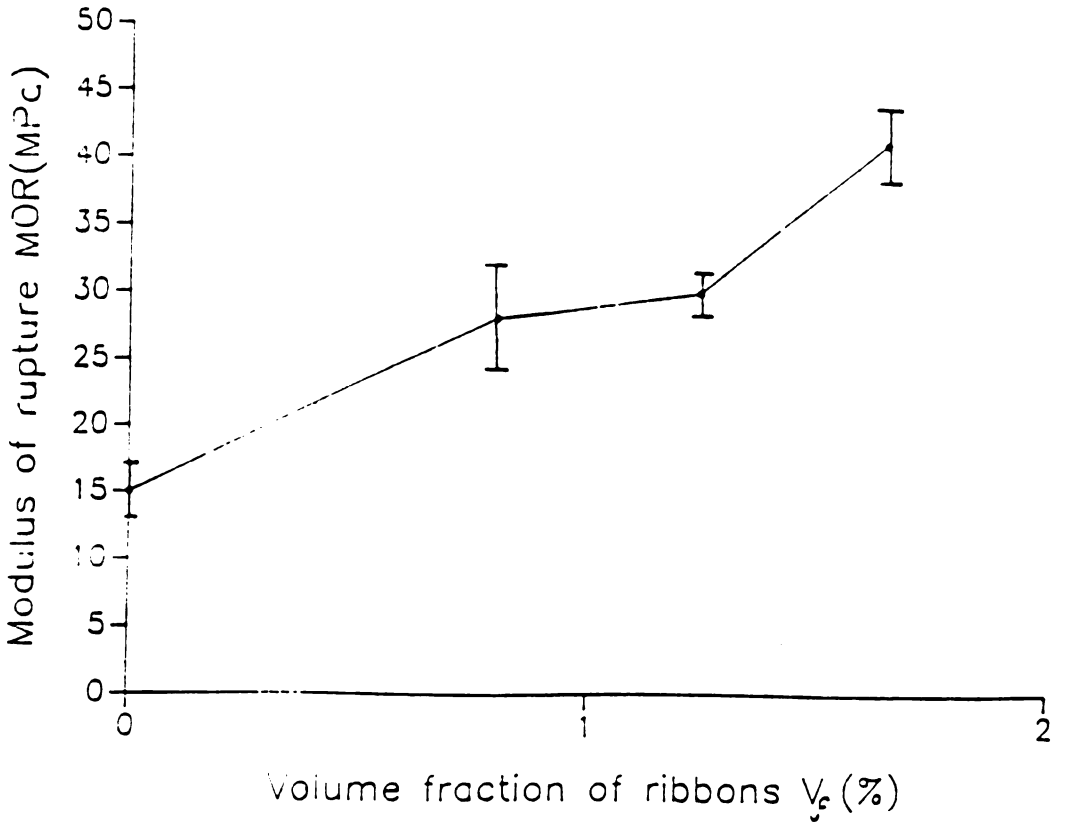

FIGURE 11. Variation in the experimentally determined fracture strength(MOR) of the composite, with increasing volume fraction of metglass ribbon reinforcement.

h is the thickness of the specimen.

In Table 8, the values of the Young's modulus obtained from the bend test, are compared with the values of the Youngs modulus obtained from the Dynamic Resonance test.

Although the values of the Young's modulus from the two different tests for the matrix agreed well, the values for the composite specimens did not. The Young's modulus for the composite specimens showed a very low value. This is because of the non-uniform load carrying characteristics of the composite, at different stages of the test. In the initial stages, the matrix carries all the load, and the deflection is small. However, once the matrix fractures, the load is transferred to the reinforcement, and the deflection obtained is larger. This large deflection manifests itself as a lower value of Young's modulus. This is further confirmed by the values of the Young's modulus obtained for the matrix specimens, which agree resonably well with the values obtained from the Dynamic Resonance technique.

The interactive effects between the fibers of a composite, play a very important role in deciding the composite properties. Kies[54] made one of the earliest quantitative estimates of the non-uniform distribution of strain in the matrix between the fibers. When a square array of reinforcing fibers(or ribbons) is subjected to a simple tensile strain, the strain magnification in the

TABLE 8. Comparison of the values of Young's modulus ofthe specimens obtained from the Dynamic Resonance test and Three point bend test:

Test	Average Young's Modulus 7572 matrix	Average Young's Modulus 7572 + MT 2605/S-2 composite
Dynamic Resonance	33.40 GPa	44.00 GPa
Three point bending	26.15 GPa	5.32 GPa

direction perpendicular to the applied stress in the matrix is given by

$$S = (2+(f_s/r))/((f_s/r)+2(E_m/E_f))$$

where, S is the strain magnification factor

f_s is the fiber spacing

r is the fiber radius(or thickness)

E_m is the Young's modulus of the matrix,

and E_f is the Youngs modulus of the fiber.

Using the values of the Young's modulus for the matrix and fiber, the fiber spacing and the fiber(ribbon) thickness, the value of S for the given composite system becomes a value nearly equal to one. This clearly indicates that the fiber interactions in the given system can be ignored.

Fractographic analysis:

A good deal of information regarding the specimen properties can be obtained by observing the fractured surfaces of the specimens. Rice[55] has provided a detailed analysis of the fractured surfaces of ceramics, and given a corelation between the material properties like fracture

toughness and the fracture features.

Under tensile or flexural loadings, the mechanical failure of ceramic bodies with limited porosity, occur due to the propagation of a single crack. The resultant fracture shows a relatively flat and smooth region, most of which is perpendicular to the tensile axis, around the initial flaw from which the failure proceeded. This flat and smooth region is called as "mirror", since in glasses(where it was first observed) it is flat and smooth enough to provide a high degree of mirror-like reflectivity. The "mirror" is bounded by "mist", which are small ridges oriented in a direction parallel to that of crack propagation. The mist region merges into larger ridges called as "hackle". These further merge into the crack branching region. These features are illustrated in Figure 12.

These features were observed on a number of specimens, which had been fractured during the bend test. In all the cases, failure was observed to originate at the tensile surface. Although the flaw, mirror and hackle regions could be differentiated easily, the mirror region was not smooth(Figures 13-16).

Although Rice[55] used the fractographic features to determine the fracture toughness of monolithic ceramics, the technique cannot be used to determine the fracture toughness of ceramic-matrix composites. This is because, the flaw initiating failure in the composite, is primarily in the

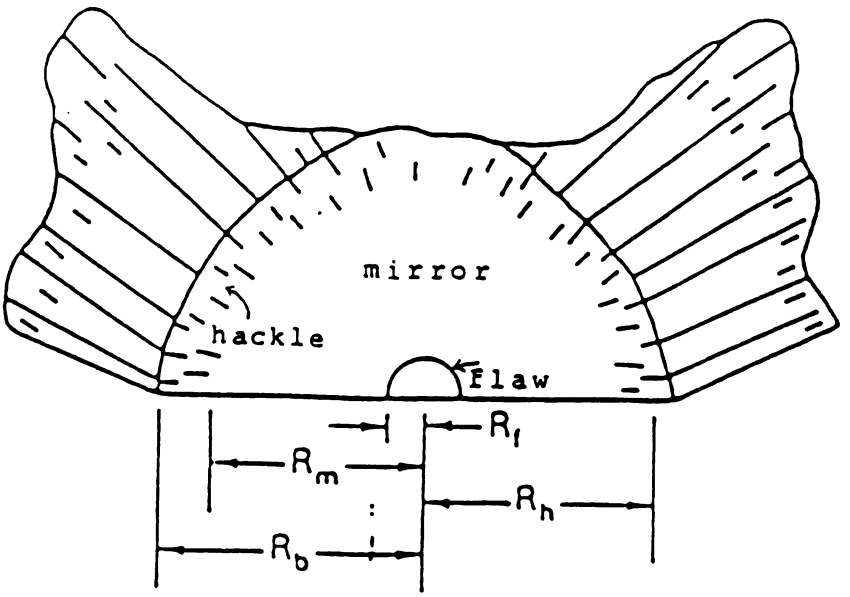

FIGURE 12. General features observed on a fractured ceramic surface[55].
R_f : flaw radius
R_m : mirror radius
R_h : hackle radius
R_b : crack branching radius.

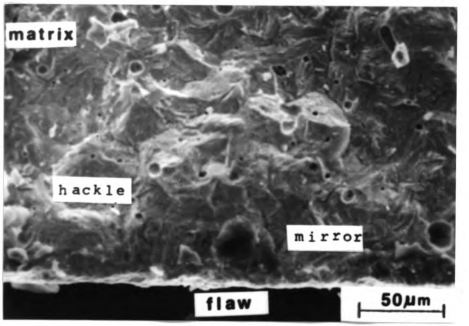

FIGURE 13. Hackle and mirror regions associated with a flaw.

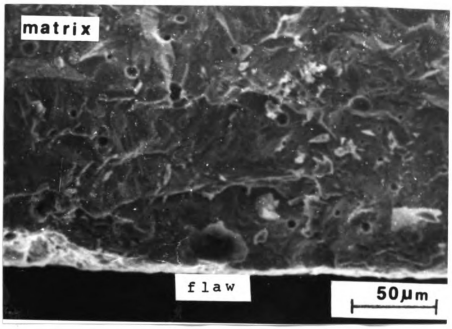

FIGURE 14. General features associated with a flaw.

FIG

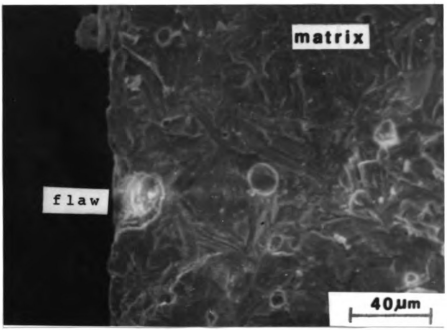

FIGURE 15. Flaw associated with the initiation of failure in the composite specimens.

FIG

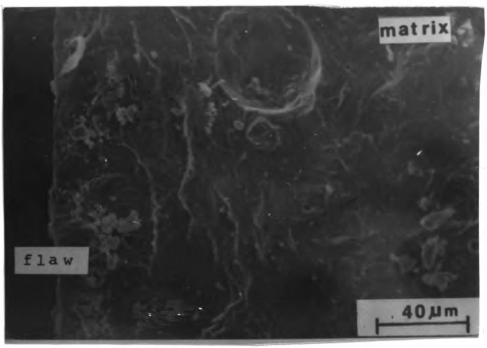

FIGURE 16. Flaw associated with the initiation of failure in the composite specimens.

mati

the

the

The

the

obta

tech

suri

stru

grai

of

obse

binc

ribb

flaw

minc

spec

of

comp

canr

ribb

expa

have

few.

matrix phase. The presence of the ribbons does not affect the initial flaw size. The ribbons only help in arresting the crack, once it begins to propagate through the matrix. The flaw size was used to evaluate the fracture toughness of the matrix, and showed good agreement with the values obtained from the Notched Beam technique and Indentation technique.

The general features observed on the fractured surfaces of various specimens were very similar. The matrix structure appeared to be 100% crystalline, with a very fine grain size. Very little porosity was observed in the matrix of the specimens. Whatever small percentage of porosity observed was probably due to incomplete evaporation of the binder during the composite fabrication.

Good bonding was observed between the reinforcing ribbons and the matrix, without the presence of any major flaws or porosity at the interface(Figures 17-20). However, minor flaws were observed at the interface, in two specimens(Figures 21-22). This could be due to the presence of dirt on the ribbons, which got incorporated into the composite during the fabrication process. Such a feature cannot be due to the thermal expansion mismatch between the ribbon and the matrix. If the flaws were due to thermal expansion mismatch between the ribbon and matrix, they would have been observed in all the specimens and not in just a few.

No ribbon pullout can be seen in any of the specimens.

FIGU

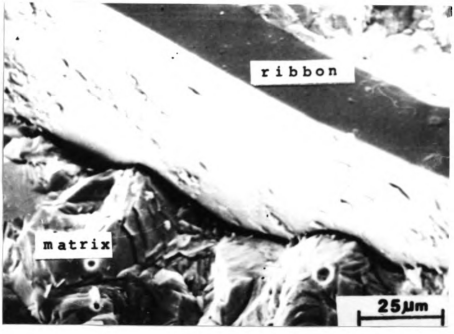

FIGURE 17. Strong interfacial bonding between the matrix and the ribbons. Some matrix material is observed to be adhering to the ribbon surface.

FIG

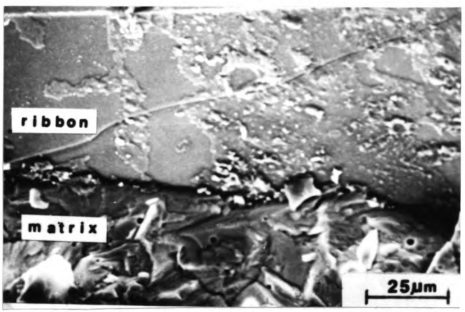

FIGURE 18. Matrix material adhering to the ribbon surface.

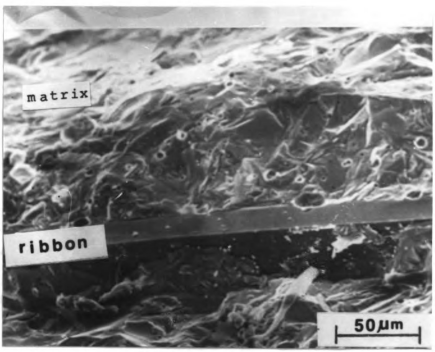

FIGURE 19. Strong(void free) bonding between the ribbon and the matrix. The matrix is observed to be 100% crystalline.

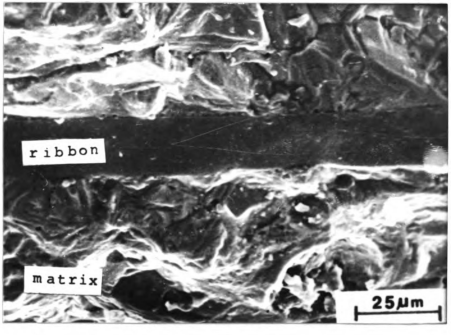

FIGURE 20. Strong(void free) bonding between the ribbon and the matrix. The matrix is observed to be 100% crystalline.

FIG

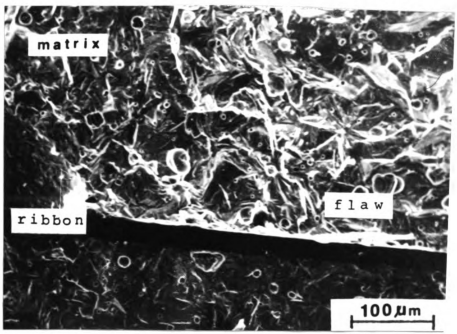

FIGURE 21. Flaw at the ribbon-matrix interface.

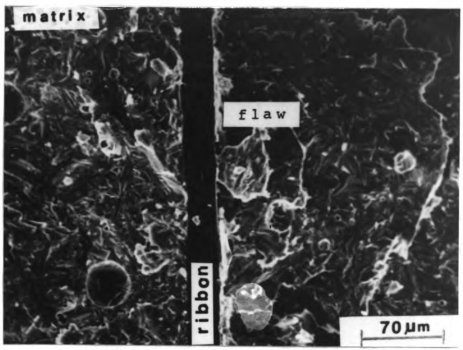

FIGURE 22. Flaw at the ribbon-matrix interface.

In Figures 17 and 18, some matrix material is observed sticking to the metglass ribbons. This is probably the matrix material which did not disengage itself from the ribbon, after the specimens were fractured in the three point bend test. This is a further evidence of the strong bonding between the ribbon and the matrix.

Microcracks were observed to originate from the edges of the reinforcing ribbons(Figures 23-24). Such a behaviour is expected, because the cross section geometry of the fibers is rectangular, and hence the corners of the ribbons act as stress concentrators. The microcracks formed were observed to deflect away from the ribbon-matrix interface, and not towards it. These microcracks could be beneficial in improving the toughness of the composite.

The ribbons were observed to be very effective in inhibiting crack propagation(Figures 25-27). Cracks which originated at the tensile surface during the bend test, were stopped by the ribbons, and deflected sideways along the ribbon-matrix interface. Crack deflection is very useful in preventing failure, and in improving the toughness of the composite system. If the interfacial bond strength could be reduced, crack deflection could weaken the interface sufficiently to cause ribbon pull-out, resulting in a dramatic increase in the fracture toughness.

The features observed in the fractured surfaces of specimens reinforced with two and three ribbons were very similar to those observed in the fractured surfaces of

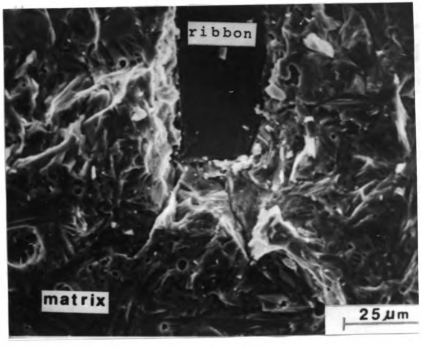

FIGURE 23. Microcracks originating at the edges of the reinforcing ribbons.

FIG

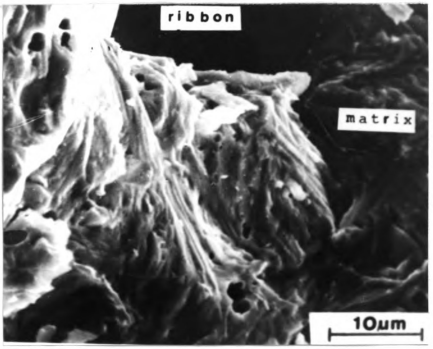

FIGURE 24. Enlarged view of a region in Figure 23. Outward propagation of the microcracks can be observed in this figure.

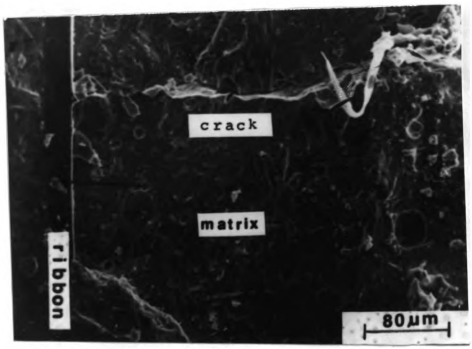

FIGURE 25. Arrest of a crack by a metglass ribbon. The crack originated at the tensile surface during the bend test.

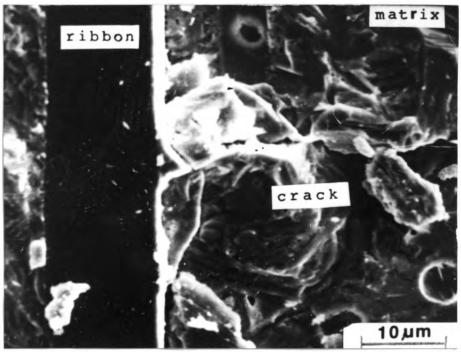

FIGURE 26. Enlarged view of a region in Figure 25. Crack arrest and deflection at the metglass ribbon-matrix interface can be observed in this figure.

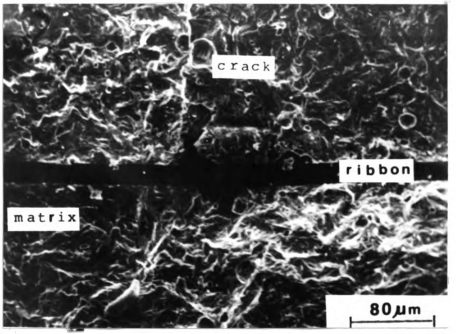

FIGURE 27. Crack arrest at the ribbon-matrix interface.

specimens reinforced with one ribbon. In specimens reinforced with one ribbon, the ribbon was located at the middle. In specimens reinforced with two ribbons, one ribbon was located below the neutral surface, while one ribbon was located above the neutral surface. The ribbon present below the neutral surface experiences tension, while the ribbon above experiences compression. Only the ribbon present below the neutral surface was effective in arresting crack propagation. By the time the crack propagates through half the specimen thickness, the specimen is overloaded, and the ribbon and matrix crack spontaneously. The case of the specimens reinforced with three ribbons was similar to the previous one, with the addition of an additional ribbon at the neutral surface. In two specimens, the presence of a "crushed zone" was observed in the vicinity of the ribbon located in the middle of the specimens(Figures 28-32).

As such, the reinforcing ribbons remained intact. However in one specimen the fractured surface of the ribbon exhibited two zones. One was smooth, while the other consisted of a veined pattern(Figure 33). The smooth region is due to local plastic shear, while the veins are produced due to localized thinning. This highly localized shear deformation results from the absence of work hardening. These type of bands were first revealed by Leamy et al[541. Some crushing was observed on one ribbon(Figure 34) in a two ribbon reinforced specimen. This was probably due to too strong a bond betwen the ribbon and matrix.

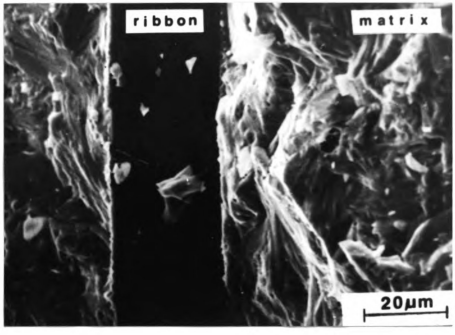

FIGURE 28. Presence of a crushed zone at the ribbon-matrix interface.

Fig

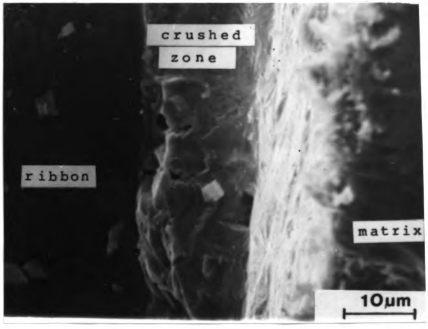

FIGURE 29. Enlarged view of a region in Figure 28. The crushed zone at the ribbon-matrix interface can be clearly seen in this figure.

FIGU

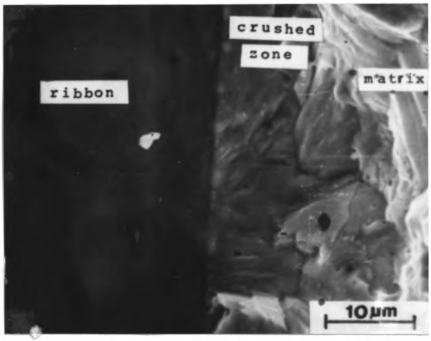

FIGURE 30. Enlarged view of a region in Figure 28.

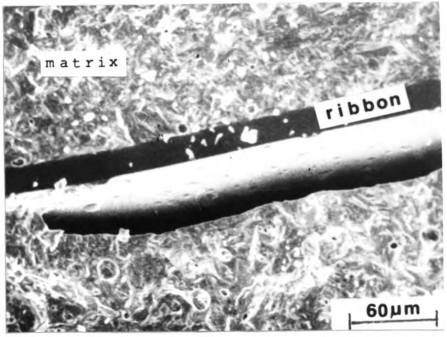

FIGURE 31. Presence of a crushed zone at the ribbon-matrix interface.

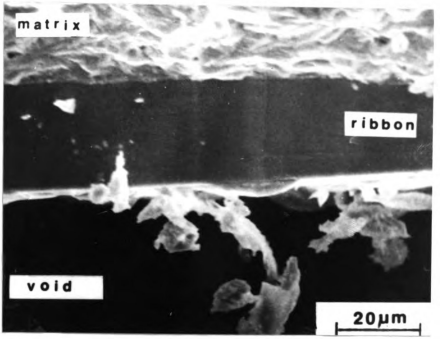

FIGURE 32. Presence of a crushed zone at the ribbon-matrix interface. Matrix material is observed to be adhering to the ribbon.

FIG

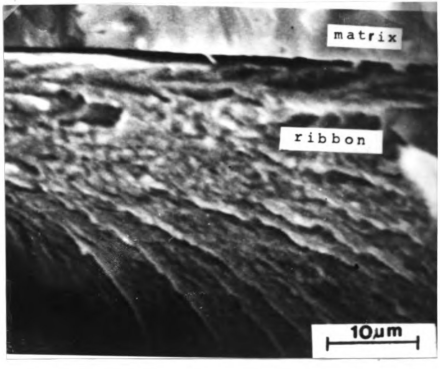

FIGURE 33. Vein type of fracture pattern on the metglass ribbon.

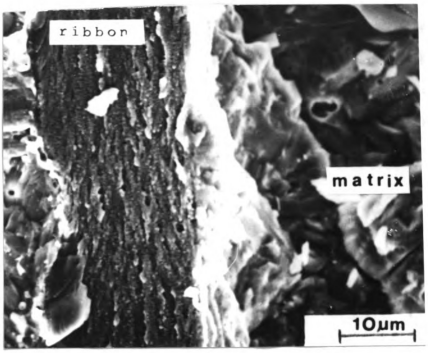

FIGURE 34. A crushed ribbon in a composite failure.

Thermal shock resistance:

The results of the thermal shock resistance test carried out on the unreinforced and composite specimes, are given in Tables 9 and 10. The effects of thermal shock on the two types of specimens are shown in the accompanying Figures 35 and 36. In general, thermal shock damage decreased the resonant frequencies in the matrix and composite specimens. The decrease in the resonance frequencies, reflect as a decrease in the modulus of elasticity. However, a variation in the trend was observed for a temperature difference of 408^{o}C. This could be attributed to two reasons. The general procedure followed in making the specimens, was to wet press the glass powder in a die, dry the green compact at 200^{o}C for 15-20 minutes to drive off the organic binder(amyl acetate), and then sinter the specimens at 400^{o}C, for about 90 minutes. After sintering, the specimens are heated to 450^{o}C for 15-20 minutes, before being furnace cooled down to room temperature. When the specimens were reheated to the testing temperature of 450^{o}C, it is possible that phase transitions occured, due to the sufficiently long exposure times. X-ray diffraction was carried out on two specimens, one which was heated to the testing temperature of 450^{o}C, and the other in its original sintered state. The X-ray

TABLE 9. Thermal shock resistance data: (unreinforced 7572 specimens)

Temperature difference	MOR(MPa)	Average MOR(MPa)	Std. deviation	Variance
158°C	15.26 12.70 20.67	16.21	4.06	25%
208°C	15.34 16.10 13.27	14.90	1.46	9.8%
258°C	11.45 13.75 8.30	11.18	2.74	24.47%
358°C	10.75 8.91 13.80	11.17	2.47	22.11%
408°C	7.53 12.93 8.60	9.70	2.86	29.50%

TABLE 10. Thermal shock resistance data:
(7572 matrix + 0.8% MT 2605/S-2 ribbons)

Temperature difference	MOR(MPa)	Average MOR(MPa)	Std.deviation	Variance
158°C	33.40 33.16 32.44	33.00	0.5	1.51%
208°C	26.58 33.20 38.83	32.87	6.13	18.65%
258°C	22.60 28.40 37.02	29.34	7.25	24.73%
358°C	20.80 17.50 10.90	16.40	5.04	30.74%
408°C	16.80 12.40 18.83	16.01	3.28	20.50%

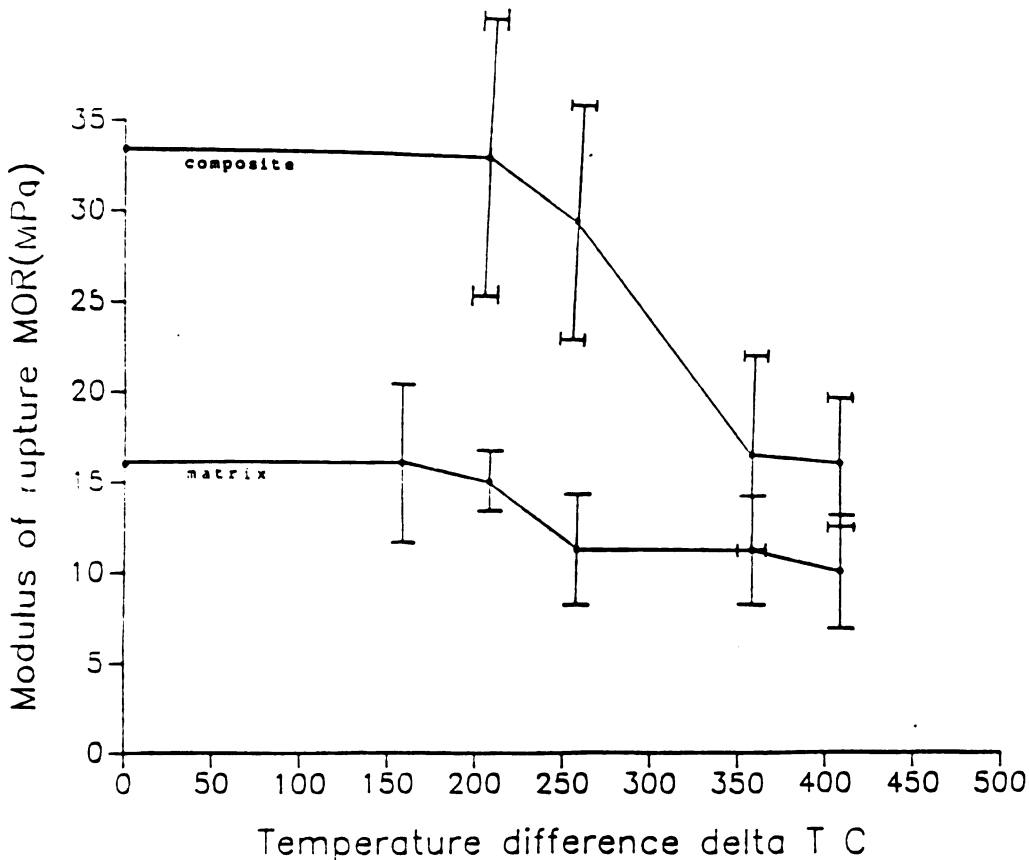

FIGURE 35. Variation in the fracture strength(MOR) with severity of quench, for the unreinforced and composite specimens.

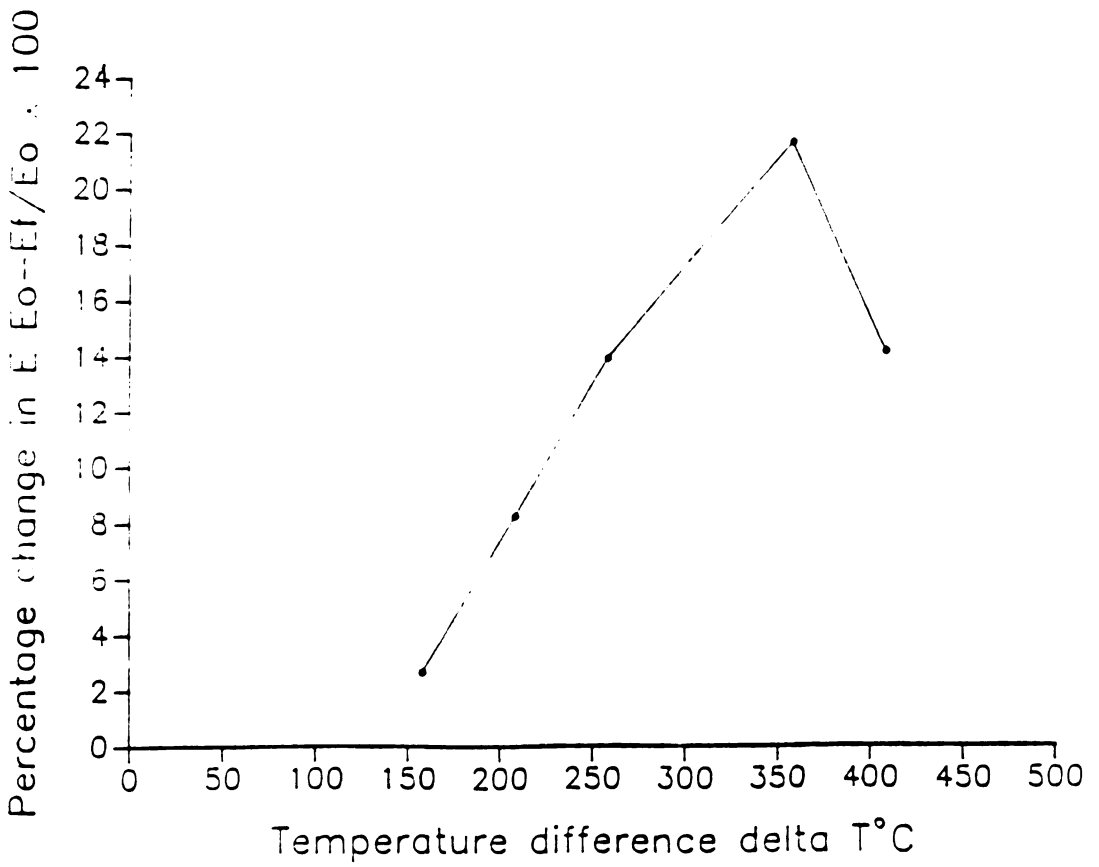

FIGURE 36. Percentage change in the Young's modulus of the unreinforced matrix specimens, with severity of quench.

diffraction results indicated the presence of additional diffraction peaks in the specimens which were reheated to the testing temperature of 450^{o}C.

The other reason could be microcrack healing. It is possible that a large number of microcracks healed up during the heating cycle, causing a reduction in the microcrack density, which in turn affects the Young's modulus. However the healing of the microcracks did not affect the strength of the specimens.

The fracture strength behaviour, on thermal shocking, is very similar to that predicted by Hasselmann[47], with some minor variations. The strength of both the matrix and composite, did not change upto a temperature difference of 200^{o}C. At temperature differences of more than 200^{o}C, the strengths of both type of specimens dropped significantly. While the fracture strength of the unreinforced specimens levelled off at about 260^{o}C, the strength of the composite specimens levelled off at about 300^{o}C. However, the drop in the strength of the composite specimens was very steep in 200^{o}-300^{o}C temperature range.

The reinforced specimens showed a slightly higher value of "critical temperature difference". The "critical temperature temperature difference " is the temperature difference corresponding to the onset of microcracking, in the thermally shocked specimens. One interesting fact to note is that the strength did not show any abnormal behaviour when quenched from the testing temperature of

450°C(which is the maximum operating temperature for the matrix). Such a behaviour can be explained on the basis that the Young's modulus reflects the effects of the total flaw spectrum over the entire specimen, where as the strength changes only result from effects on the critical flaws. It is unlikely that the critical flaws had time to heal up during these short exposure times.

Another important consideration is the effect of the reinforcements on the thermal shock resistance. As stated earlier, the reinforced specimens exhibited a "critical temperature difference" only slightly higher than that of the matrix specimens. Ribbon location within the matrix is an important aspect, and needs to be considered. The composite samples tested, had a single ribbon located at the center of the specimen. During quenching, it is obvious that the surface cools at a much faster rate than the interior. Since it cools faster, it also shrinks faster. But, the interior inhibits this shrinkage and causes tensile stresses to develop in the surface, while compressive stresses develop in the interior. As the interior cools, it begins to shrink too, thus releasing the tensile stresses on the surface. If the specimens were thick enough, it is possible that the contraction of the interior could lead to a reversal of stress states, causing the surface to be in a state of compression and the interior in a state of tension. However, the specimens tested in the present study were very thin. Hence the surface is in a state of residual tension,

while the interior is in a state of residual compression. In this case the stresses due to thermal expansion mismatch between the ribbons and the matrix can be neglected, since the coefficient of thermal expansion of the two component phases is almost the same. Also, these stresses are highly localized at the interface because of the very small volume fraction and small thickness of the metglass ribbons.

There are tensile stresses on the surface, followed by a region of compressive stresses in the interior. Cracks generated at the surface during thermal shock, tend to propagate more readily through the tensile stress field present near the surface[57]. As the cracks propogate into the specimen, they encounter the compressive stress field, and are deflected back into the tensile stress field located near the surface. This can be clearly seen in Figures[37-41].

Hence the ribbon plays no part at all in inhibiting crack growth, during thermal shocking. The positioning a single ribbon at the neutral surface does not help in improving the thermal shock resistance. The higher strength of the composite specimens is because of crack arrest by the ribbon during the bend test. The thermal shock resistance of the composite could be improved by increasing the volume fraction of the metglass ribbon reinforcement, and by positioning the ribbon close to the surface experiencing tensile stress.

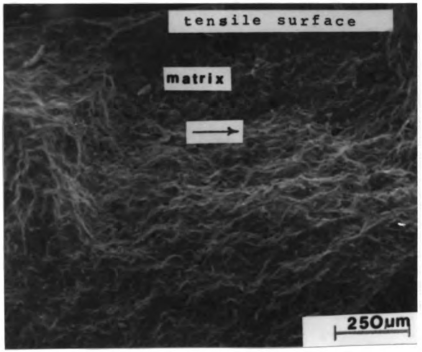

FIGURE 37. Crack deflection into the tensile region of the thermally shocked specimens.

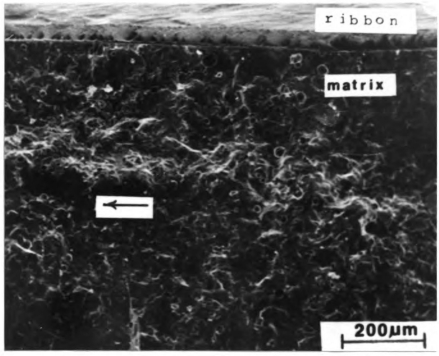

FIGURE 38. Crack deflection into the tensile region of the thermally shocked specimens.

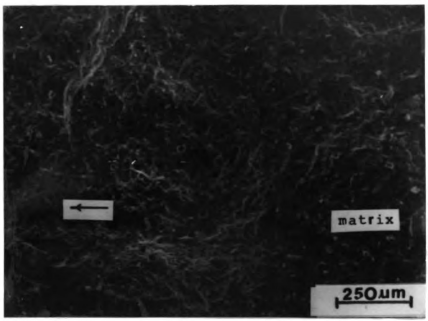

FIGURE 39. Crack deflection into the tensile region of the thermally shocked specimens.

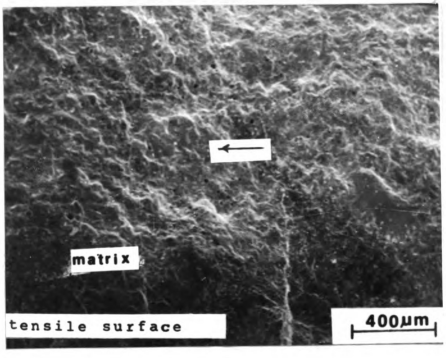

FIGURE 40. Crack deflection into the tensile region of the thermally shocked specimens.

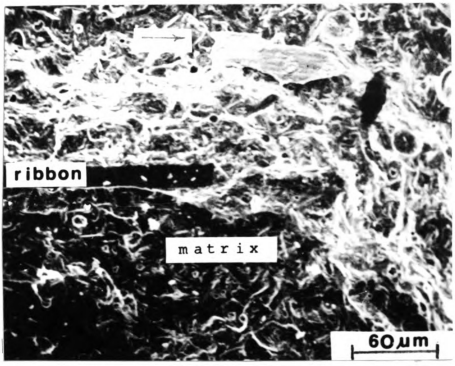

FIGURE 41. Crack deflection and branching arond the metglass ribbons in the thermally shocked specimens.

Fracture toughness measurements:

The values of the fracture toughness for the matrix and the composite specimens, as measured by the two techniques, are given in Tables 11 and 12. It is clearly evident that introduction of even a very small volume fraction of metglass ribbons, causes a dramatic improvement in the fracture toughness. The variation in the fracture toughness of the composite specimens, with increasing volume fraction of metglass reinforcement, is illustrated in Figure 42 With a percent volume fraction reinforcement of just 1.64%, an improvement in the toughness of more than 300% can be obtained. With the incorporation of higher percentages of volume fraction reinforcements, the toughness of the composite specimens could be improved dramatically.

The value of the fracture toughness of the matrix as obtained from the indentation technique, was higher than the value obtained from the destructive notched-beam technique. This could be attributed to a larger number of mechanical, instrumental and human errors involved in measuring the toughness by the notched beam technique.

TABLE 11. Results of the Notched Beam test used in the measurement of Fracture toughness:

Sample	K_{IC} ($MPam^{1/2}$)	Average K_{IC} ($MPam^{1/2}$)	Std. Deviation	Variance
7572 matrix	0.4046 0.3580 0.3730	0.378	0.0237	6.26%
7572 matrix reinforced with 0.6% MT 2605/S-2 (one fiber)	1.0886 0.8320 1.1800 0.7080	0.952	0.3022	31.74%
7572 matrix reinforced with 1.24% MT 2605/S-2 (two fibers)	1.372 1.430	1.401	0.041	2.93%
Thermally shocked specimen				
7572 matrix temperature difference 408°C.	0.200 0.119	0.16	0.0573	35.81%

TABLE 12. Results of the Indentation technique used for the measurement of Fracture toughness:

Specimen :	Lead Borosilicate glass, code 7572.	
Indentation load :	0.3 Kg.	
Loading time:	20 seconds.	
Loading speed :	50 micometers/sec.	
Number of specimens :	3	
Indentations per specimen :	25	
Fracture toughness :	0.496	
	0.433	Average : 0.46
$K_{IC}(MPam^{1/2})$	0.450	
Standard deviation :	0.0327	
Variance :	7.11%	

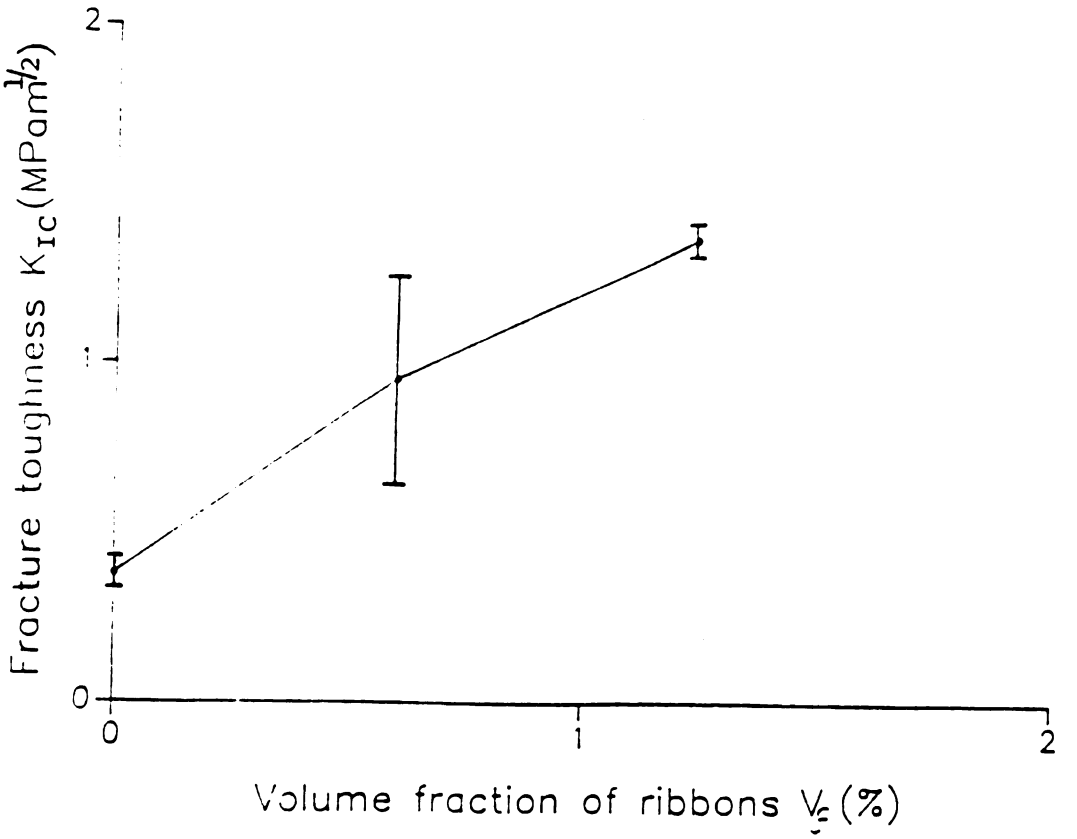

FIGURE 42. Variation in the fracture toughness(K_{IC}) with increasing volume fraction of metglass ribbon reinforcement.

Interfacial bond strength:

During these studies, all the specimens exhibited fiber failure, with no pullout. This is indicative of a very strong bond between the metglass ribbons and the matrix. Since the fiber-matrix bond is extremely strong, the resultant flaw causing failure is mainly in the matrix phase.

Another approach to measure the bond strength, is to test the composite in such a way, that failure occurs in a shear mode, parallel to the fibers[51]. The three point bend test can be used for producing such conditions. The shear stresses on the midplane are related to the applied load as,

$$T = (3P)/(4bd)$$

where, T is the interfacial bond strength
P is the load at failure
b is the width of the specimen, and
d is the specimen thickness.

For the same specimen and test geometry, the maximum tensile stress parallel to the ribbons, which occurs at the midpoint on the outer ribbon, in the tensile surface, is

given by,

$$\sigma = (3PL)/(2bd^2).$$

The results from the three point bend test were used in evaluating the midplane shear stress. The results for the midplane shear stress and Modulus of rupture are given in Table 13. It is clearly evident that the interfacial bond strength between the fiber and matrix is very high. This is confirmed from the calculated values of the ratios of the midplane shear stress to the Modulus of Rupture. This phenomenon can also be observed in Figures 17-20.

TABLE 13. MOR and midplane shear stress for the matrix and composite specimens:

Ceramic Glass matrix	Metglass reinforcement	MOR MPa	T MPa	T/MOR
7572	-	14.98	0.9528	0.0636
8463	-	11.30	0.5640	0.0499
7572	MT 2605 /S-2	28.25	2.3510	0.0804

CONCLUSIONS

1. It is feasible to use metglass ribbons as reinforcements for brittle glass-ceramic matrices. Such composites can be processed by low cost techniques such as wet-pressing and sintering, provided a right selection of the component phases of the composite system is made.

2. Even small volume fractions of the metglass ribbon reinforcements, significantly improve the strength, elastic properties and fracture toughness of the glass-ceramic matrices.

3. The rule of mixtures which is used to characterize the elastic properties of various composite systems, cannot be used in the case of the metglass reinforced glass-ceramic system. A better estimation of the Young's modulus can be made by fitting the experimentally obtained values to the equations suggested by Halpin and Tsai[52].

4. The strength of the metglass reinforced glass-ceramic composites, is primarily controlled by the strength of the reinforcing metglass ribbons, and is a function of the volume fraction of the reinforcing metglass ribbons.

5. The fracture toughness of such metglass reinforced glass-ceramic composites, could be improved by controlling the microcracking occuring at the edges of the reinforcing metglass ribbons.

6. The interfacial bond between the metglass ribbon reinforcements and glass-ceramic matrix, is very strong.

7. A single metglass ribbon reinforcement, placed in the middle of the specimen, does not significantly change the thermal shock resistance of the glass-ceramic matrix.

REFERENCES:

1. R. Sambell, D. Brown and D. Phillips, "Carbon fiber composites with ceramic and glass matrices", part 1: discontinuous fibers, J. Mat. Sci., 7 (1972) 663-675.

2. R. Sambell, D. Brown and D. Phillips, "Carbon fiber composites with ceramic and glass matrices", part 2:continuous fibers, ibid, 7 (1972) 676-681.

3. M. Sahebkar, J. Schlichting and P. Schubert, "Possibility of reinforcing glass with carbon fibers", Berichte de Deutschen Keramischen Gesellschaft, 55 (1978) 265-268.

4. K. Faber and A. Evans, "Crack deflection processes-1 Experiment ", Acta Metall., 31 (1983) 565-576.

5. K. Faber and A. Evans, "Crack deflection processes-2 Experiment ", 1bid, 31 (1983) 577-584.

6. K. Faber and A. Evans, "Intergranular crack deflection toughening in Silicon carbide", J. Am. Cer. Soc., 66 (1983) 94-96.

7. K. Faber and A. Evans, "Crack growth resistance of microcracked brittle materials", J. Am. Cer. Soc., 67 (1984) 255-260.

8. A. Evans and A. Heuer, "Review of the transformation toughening in ceramics -martensitic transformation in crack tip fields", J. Am. Cer. Soc., 63 (1980) 241-248.

9. A. Evans, "Toughening mechanisms in zirconia alloys", in "Advances in ceramics", Vol. 12, Edited by N. Claussen, M. Ruhle and A. Heuer, Am. Cer. Soc., Ohio 1984, p 193-212.

10. R. McMeeking and A. Evans, "Mechanics of transformation toughening in brittle materials", J. Am. Cer. Soc., 65 (1982) 242-246.

11. D. Marshall, B. Cox and A. Evans, "The mechanics of matrix cracking in brittle matrix fiber composites", Acta Metall., 33 (1985) 2013-2021.

12. R. Steinbrech, R. Khehans and W. Schaarwachter, "Increase in the crack resistance during slow crack growth in alumina bend specimens", J. Mat. Sci., 18 (1983) 265-270.

13. B. Lawn, "The indentation crack as a model surface flaw", in "Fracture mechanics of ceramics" Vol.5, Edited by

R. Bradt, A. Evans and D. P. H. Hasselmann, Plenum press, New York, 1983, p 1-25.

14. D. Shetty, A. Rosenfield and W. Duckworth, "Analysis of an indentation crack as a wedge loaded half penny crack", J. Am. Cer. Soc., 68 (1985) 65-67.

15. D. Marshall, "Controlled flaws in ceramics:A comparison of the Knoop and Vickers indentation", J. Am. Ceram. Soc., 66 (1983) 127-131.

16. B. Lawn, A. Evans and D. Marshall, "Elastic-plastic indentation damage in ceramics:The median/radial crack system", J. Am. Cer. Soc., 63 (1980) 574-581.

17. D. Marshall, "Surface damage in ceramics:Implications for strength degradation, erosion and wear", in "Nitrogen ceramics" edited by F. Riley, Nijhoff, The Hague, 1983, p 635-656.

18. T. Dabbs, D. Marshall and B. Lawn, "Flaw generation in glass fibers", ibid, 63 (1980) 224-225.

19. W. Hillig, " Prospects for ultra high temperature ceramics", Proc. conf. on tailoring multiphase and composite ceramics, Pennsylvania, July 1985, in press.

20. A. Evans, "Microfracture from thermal expansion anisotropy", Acta Metall., 26 (1978) 1845-1853.

21. R. Rice, J. Spann and W. Coblenz, "The effect of ceramic fiber coatings on the room temperature mechanical behaviour of ceramic fiber composites", Ceram. Eng. Sci. Proc. 5 (1984) 614-624.

22. B. Bender, D. Lewis and R. Rice, "Electron microscopy of ceramic fiber ceramic matrix composites", ibid, 513-529.

23. D. Marshall and A. Evans, "Failure mechanisms in ceramic fiber-ceramic matrix composites", J. Am. Cer. Soc., 68 (1985) 225-231.

24. K. Gadkaree and K. Chyung, "Silicon carbide whisker reinforced glass and glass-ceramic composites", Am. Cer. Soc. Bul., 65 (1986) 370-376.

25. P. Shalek, J. Petrovik and F. Gac, "Hot pressed silicon carbide-silicon nitride matrix composites", Am. Cer. Soc. Bul., 65 (1986) 351-356.

26. S. Risbud and M. Herron, " Characterization of silicon carbide fiber reinforced Ba-Si-Al-O-N glass-ceramic composites", Am. Cer. Soc. Bul., 65 (1986) 342-346.

27. J. Homeny, W. Vaughn and M. Ferber, "Processing and mechanical properties of silicon carbide whisker alumina matrix composites", Am. Cer. Soc. Bul., 67 (1987) 333-338.

28. T. Tiegs and P. Becher, "Sintered alumina silicon carbide whisker composites", Am. Cer. Soc. Bul., 66 (1987) 339-342.

29. S. Bulijan, G. Baldoni and M. Huckabee, "Silicon carbide-silicon nitride composites", Am. Cer. Soc. Bul., 66 (1987) 347-352.

30. A. Caputo, D. Stinton and T. Besmann, " Fiber reinforced silicon carbide composites with improved mechanical properties", Am. Cer. Soc. Bul., 66 (1987) 368-372.

31. Y. Hasegawa, M. Iimara and S. Yajima, " Synthesis of continuous silicon carbide fibers by the conversion of polycarbosilane", J. Mat. Sci. 15 (1980) 720-728.

32. D. Seyferth and G. Wiseman, " High yield synthesis of silicon carbide and silicon nitride ceramics, by pyrolysis of a novel ploy organosilane", J. Am. Cer. Soc., 67 (1984) 132-133.

33. W. Coblenz, G. Wiseman, D. Davis and R. Rice, " Emergent process methods for high technology ceramics", edited by R. Davis, H.Palmour and R.Porter, Plenum press, New York, 1984, p 271-285.

34. J. Lanutti and R. Clark, " Better ceramics through chemistry", Edited by C. Brinker, D. Clark and D. Ulrich, North Holland press, 1984, p 369-381.

35. H. Chen and D. Turnbull, " A Pd-Si metglass", J. Chem. Phy., 48 (1968) 2560-2571.

36. R. Dann, "Glass like metals cut cost and energy use", "Machine design" by Penton publishers, New York, April 26, 1984, p 1-12.

37. J. C. M. Li, " Mechanical properties of amorphous metals and alloys", in "Treatise on material science and technology, Vol.20:Ultrarapid quenching of liquid alloys", Edited by H. Hermann, Academic press, New York, 1981, p 326-389.

38. L. Davis, "Metallic glasses", A.S.M. Seminar, Niagara Falls, 1978, p 190-223.

39. T. Masmuto and R. Maddin, "Mechanical properties of

metallic glasses", Acta. Metall., 19 (1971) 725-741.

40. A. Fels, K. Friedrich and E. Hornbogen, "Reinforcement of a brittle epoxy resin by metallic glass ribbons", J. Mat. Sci. letters 3 (1984) 569-574.

41. A. Fels, E. Hornbogen and K. Friedrich, "A study of the reinforcement by prestressed metallic glasses", J. Mat. Sci. letters 3 (1984) 639-642.

42. T. Tio, K. Friedrich, E. Hornbogen, U. Koster and A. Fels, "Pullout tests with metallic glass ribbons, in different matrices", J. Mat. Sci. letters 3 (1984) 415-419.

43. M. Lasocka and H. Matyja, "Annealing effect in Metallic glasses", in "Treatise on material science and technology, Vol.20:Ultrarapid quenching of liquid alloys", Edited by H. Hermann, Academic press, New York, 1981, p 261-286.

44. S. Screiber, D. Anderson and N. Soga, "Dynamic resonance method for measuring the elastic modului of solids", Chp.4 from "Elastic constants and their measurements", McGraw Hill, New York, 1974, p 82-125.

45. E. Case, private communications.

46. M. Srinivasan and S. Seshadri, "Application of the single edge notched beam and indentation technique to determine the fracture toughness of alpha-silicon carbide", from "Fracture mechanics for ceramics, rocks and concrete", ASTM special publication Nos. 745, 1977, p 46-69.

47. D. P. H. Hasselmann, "Thermal stress crack stability and propogation in severe thermal environments" from "Ceramics in severe environments", Material Science Research , Vol.5, Edited by W. Kriegel and H. Palmour, Plenum press, New York, 1972, P 89-105.

48. D. Lewis, "Thermal shock and thermal shock fatigue testing of ceramics with the water quench test", in "Fracture mechanics of ceramics", Vol. 6 edited by A. Evans, D. P. H. Hasselmann and F. Lange, Permagnon press, New York 1984, p 487-496.

49. J. R. G. Evans, R. Stevens and S. Tan, "Thermal shocking of alumina", J. Mat. Sci. 19 (1984) 3692-3701.

50. G. Bansal and W. Duckworth, " Fracture surface energy measurements by the notched beam technique", Proceedings of the 11th national ASTM symposium on fracture mechanics.

51. D. Hull, " Measurement of the bond strength in composites", Chp.3 from "An introduction to composite materials", Edited by R. Cahn, E. Davis and I. Ward, Cambridge University press, Cambridge, 1985, p 48-57.

52. J.Halpin and S.Tsai, "Environmental factors in composite material design", Air Force Materials Laboratory Technical Report AFML-TR-67-423, 1967.

53. D. Hull, "Longitudional tensile strength of composites", Chp.7 from "An introduction to composite materials", Edited by R. Cahn, E. Davis and I. Ward, Cambridge University press, cambridge, 1985, p 127-142.

54. J. Kies, "Maximum strains in the resin of fiberglass composites", from United States Naval Research Report NRL 5752, 1962.

55. R. Rice, " Ceramic fracture features, observations, mechanisms and uses", ASTM Special technical publication Nos.827 (1984) p 5-103.

56. H. Leamy, H. Chen and T. Wang, Metallurgical transactions 3 (1972) 699-708.

57. H. Kamizono and K. Niwa, "An estimation of the thermal shock resistance of simulated nuclear waste glass under water quenching conditions", J. Mat. Sci. letters, 3 (1984) 588-590.